Research Reports on Computer Science
https://ojs.wiserpub.com/index.php/RRCS/

UNIVERSAL WISER PUBLISHER

Research Article

Digital Simulations for Three-dimensional Nonlinear Advection-diffusion Equations Using Quasi-variable Meshes High-resolution Implicit Compact Scheme

Navnit Jha[1*], **Ping Lin**[2]

[1]Department of Mathematics, South Asian University, New Delhi, India
[2]School of Science and Engineering, University of Dundee, Dundee, Scotland, United Kingdom
E-mail: navnitjha@sau.ac.in

Received: 8 April 2022; **Revised:** 13 May 2022; **Accepted:** 23 May 2022

Abstract: A two-level implicit compact formulation with quasi-variable meshes is reported for solving three-dimensions second-order nonlinear parabolic partial differential equations. The new nineteen-point compact scheme exhibit fourth and second-order accuracy in space and time on a variable mesh steps and uniformly spaced mesh points. We have also developed an operator-splitting technique to implement the alternating direction implicit (ADI) scheme for computing the 3D advection-diffusion equation. Thomas algorithm computes each tri-diagonal matrix that arises from ADI steps in minimal computing time. The operator-splitting form is unconditionally stable. The improved accuracy is achieved at a lower cost of computation and storage because the spatial mesh parameters tune the mesh location according to solution values' behavior. The new method is successfully applied to the Navier-Stokes equation, advection-diffusion equation, and Burger's equation for the computational illustrations that corroborate the order, accuracies, and robustness of the new high-order implicit compact scheme. The main highlight of the present work lies in obtaining a fourth-order scheme on a quasi-variable mesh network, and its superiority over the comparable uniform meshes high-order compact scheme.

Keywords: compact scheme, ADI method, quasi-variable mesh network, advection-diffusion equation, Navier-Stokes equation, Burger's equation, stability

1. Introduction

The necessity for understanding the partial differential equations in modeling the physical phenomenon has observed tremendous growth in mathematical theory and attracted physicists, engineers, and mathematicians. The three-dimensional advection-diffusion equations (ADEs) are used to describe several circumstances such as convection-diffusion, air pollution, fluid flow, heat exchange, image processing, and mass transfer. The heat conduction equation, Burger's equation, air pollutant transport model, and Navier-Stokes equations are some of the essential mathematical models that appear in modeling ocean currents, airflow around a wing, blood flow, and design of power stations. The 3D diffusion-advection model appears in river thermal pollution, transport in semiconductor devices, heat transfer in a draining film charge, fluid flow in porous media, contaminant dispersion in shallow water, and atmospheric pollutant transport [1, 2]. Advection-diffusion-reaction response model arrangements with time advancement in biological species or substances in a blowing medium, for example, air and water [3]. Many such mathematical models do not

DOI: https://doi.org/10.37256/rrcs.1120221466

possess analytic solutions; therefore, numerical analysis of multi-dimensional ADEs is of great interest to engineers and scientists. The available computational techniques lack optimal memory, efficiency, and numerical accuracy of discrete solution values. This is because the resulting nonlinear discrete equations are large enough and restrain the implementation to conventional computers due to limited computing time and inadequate memory storage. Therefore, developing stable, efficient, and accurate numerical schemes for determining approximating solution values of ADEs is vital. Researchers may have made an excellent effort to construct a high-order scheme due to computational efficiency and reasonable accuracy [4-6]. In recent years, compact finite-difference discretization has been delineated for linear time-dependent convection-diffusion equations in [7-11]. Karaa and Othman [12] described a two-level high-resolution difference method to obtain the numerical approximations of three-dimensional ADEs with mixed derivatives. Mohanty and Setia [13] described an off-step fourth-order method for time-dependent three-dimensional quasi-linear ADEs, and the proposed scheme applies to cylindrical and spherical polar coordinates. A three-dimensional micro heat transfer model is solved using the local one-dimensional method in [14]. Based on Pade-approximations, the high-order finite-difference method combined with the unconditional stable alternating direction implicit (ADI) scheme is obtained for a three space dimensions reaction-diffusion model along with Neumann boundary data [15]. A single cell compact discretization of accuracy two and four in time and space, respectively, to the normal derivative appearing in three-dimensional quasi-linear ADEs, was developed in [16]. The mathematical analysis and computational illustrations associated with a fractional form of ADE, Navier-Stokes equation, Burger-Huxley equation, and reaction-diffusion equation have been analyzed in [17-26].

Literature related to multi-dimension partial differential equations is mainly devoted to uniform mesh step-sizes, and non-uniform meshes were given less attention. The straightforward implementation of finite-difference discretization produces approximate solution values using direct or iterative methods, and with a long run time, one can achieve almost exact solution values. The standard finite-difference approximations work well with smooth solutions but can give oscillatory or unbounded numerical results when perturbations are introduced [27, 28]. This is because truncation errors and discretization errors emanating from taking a finite number of computation steps to approximate are infinite. The local truncation errors in the discretization rely on the step-size of meshes and derivative of the variable. The presence of first-order spatial derivative (viscosity) in truncation error usually causes trouble and may destroy solutions [29]. Therefore, uniform meshes often yield a non-uniform distribution of errors. The implementation of non-uniform meshes tackles such variations in the error. The smaller mesh step-size in the sub-domain where the derivative of the function value is enormous. Larger step size in the sub-domain where the value of function derivative is small and thus results in uniform distribution of discretization errors. In this way, we may have a uniform distribution of truncation errors over the integration domain and obtain a more precise resolution to a pre-assigned quantity of meshes. Some additional features emerged using non-uniform meshes in simulations [30, 31].

The beauty of high accuracy numerical schemes for simulation is fully recognized for the fundamental fluid flow. High-order finite-difference discretizations have low dispersion and require a significantly reduced number of mesh points to ensure tolerable levels of numerical error. Non-compact finite-difference discretization requires a wide number of computational stencils as the order of approximation increases. These large stencils are challenging to handle at the boundary where no data is available to perform differencing. Also, large stencils result in high bandwidth of matrix whose inversion is computationally costly. Therefore, the high-order finite-difference discretization on compact stencils solves such complications. Compact stands for the numerical scheme with minimal stencil width. Non-uniform meshes allow mesh points to be more refined in the sub-domain where stiff gradients are expected. Finite-difference discretization of partial order derivatives in the ADEs are essential to constitute a stable, accurate, and computationally proficient scheme with minimum numerical dissipation and dispersion. In the present work, we describe a high-order accurate implicit compact scheme to the mildly nonlinear time-dependent ADEs of the form

$$\epsilon(W^{xx}+W^{yy}+W^{zz}) = G(x,y,z,t,W,W^{x},W^{y},W^{z},W^{t}),\ (x,y,z,t)\in\Omega, \tag{1}$$

where $\Omega=\{(x,y,z,t): 0<x,y,z<1, 0<t<T\}$, $0<\epsilon\ll 1$, $W=W(x,y,z,t)$, $W^{x}=\partial W/\partial x$, $W^{xx}=\partial^2 W/\partial x^2$, etc. and associated initial and boundary values are assigned as

$$W(x,y,z,0)=K_0(x,y,z), 0\le x,y,z\le 1, \tag{2}$$

$$\left.\begin{matrix} W(x,y,0,t)=K_5(x,y,t) \\ W(x,y,1,t)=K_6(x,y,t) \end{matrix}\right], 0 \le x,y \le 1, \tag{3}$$

$$\left.\begin{matrix} W(0,y,z,t)=K_1(y,z,t) \\ W(1,y,z,t)=K_2(y,z,t) \end{matrix}\right], 0 \le y,z \le 1, \tag{4}$$

$$\left.\begin{matrix} W(x,0,z,t)=K_3(x,z,t) \\ W(x,1,z,t)=K_4(x,z,t) \end{matrix}\right], 0 \le x,z \le 1, t > 0. \tag{5}$$

The mathematical examination of an incredibly enormous class of time-dependent partial differential equations (PDEs) having nonlinear first-order spatial and temporal derivatives is vital due to the absence of a theoretical solution in general. The proposed discretization procedure yields finite linear algebraic systems having sparse matrix structures, and therefore, iterative methods are suitable. In Sections 2 and 3, we shall describe mesh topology, compact operators, and the formulation of a numerical scheme that falls within the scope of optimum accuracy. Section 4 describes an alternating direction iterative scheme as experimented with the 3D time-dependent convection-diffusion model. An extension of the proposed numerical scheme to the coupled Burger's equations and details of unconditional stability is given in Section 5. Numerical simulations with linear and nonlinear problems are performed in Section 6 using non-uniform and uniform meshes optimum-order compact scheme. The approximate and exact solution values are compared regarding maximum absolute errors and numerical convergence order. The paper is finally concluded with observations and possible extensions.

2. Quasi-variable mesh network

Non-uniform mesh steps are commonly applied to improve numerical solution values' accuracy for the discretized partial differential equation whose solutions are not smooth. One such non-uniform mesh spacing in one-dimension is three-point discretization, wherein the next mesh step-size has nonlinear relation to the previous mesh-step size. In the present scenario, the solution domain $\Omega = \{(x,y,z,t): 0 \le x,y,z \le 1, 0 \le t \le T\}$ is partitioned into the mesh points $\{(x_l, y_m, z_n, t_j), 0 \le l \le L+1, 0 \le m \le M+1, 0 \le n \le N+1, 0 \le j \le J\}$. The time-step $\Delta t = T/J$ is fixed and temporal mesh points are $t_j = j\Delta t, \ 0 \le j \le J$. Let $\Delta x_l = x_l - x_{l-1}, l = 1(1)L+1, \Delta y_m = y_m - y_{m-1}, m = 1(1)M+1$ and $\Delta z_n = z_n - z_{n-1}, n = 1(1)N+1,$ be the step-sizes in spatial directions. The following step sizes are defined by

$$\Delta x_{l+1} = \Delta x_l(1+p\Delta x_l), \Delta y_{m+1} = \Delta y_m(1+q\Delta y_m), \Delta z_{n+1} = \Delta z_n(1+r\Delta z_n), l = 1(1)L, m = 1(1)M, n = 1(1)N, \tag{6}$$

where the mesh-expansion ratios $p,q,r \in (0,1)$. In particular, when p = 0, q = 0, or r = 0, it produces a uniform distribution of mesh points along x-, y- or z-directions. In order to generate numerical mesh points, we shall use normalization parameters to the mesh-step sizes as $\Delta x_{l+1} = \Delta x_l(1+p\Delta x_l/\Delta x_1), l = 1(1)L$ and as the length of the spatial domain in each direction is unity, thus, $\Sigma_{l=1}^{L+1}\Delta x_l = 1$. As a result, for the known value of mesh-expansion parameter p and boundary mesh points x_0 = 0, x_{L+1} = 1, we can generate the quasi-variable mesh step-length and corresponding internal mesh points according to the formula a_1 = 1, a_2 = 1 + p, a_{l-1} = (1 + pa_{l-1}), l = 3 (1) L + 1, $\Delta x_1 = (x_{L+1} - x_0)/\Sigma_{l=1}^{L+1}\Delta a_l$, $\Delta x_2 = \Delta x_1 a_2, \Delta x_l = \Delta x_1 a_l, l = 3(1)L+1, x_l = x_{l-1} + \Delta x_l, l = 1(1)L$. Similarly, we can generate y- and z-space mesh points for the known value of boundary mesh points and mesh-expansion parameters q and r respectively. For p ≥ 0, we find that $\Delta x_{l+1} \ge \Delta x_l$ for all l, thus, the mesh-step sequence $\{\Delta x_l\}_{l=1}^{L+1}$ is monotonic increasing. Therefore, there is a Lagrange interpolating polynomial ψ having degree $L+1$ and $\psi(x_l^*) = x_l, l = 0, ..., \overline{L+1}$, where $\{x_l^* = l\Delta x, l = 0, ..., \overline{L+1}, \Delta x = 1/(1+L)\}$ is the uniform partition of the interval [0,1]. By using the mean value theorem, one obtains

$$\Delta x_{l+1} = x_{l+1} - x_l = \psi(x_{l+1}^*) - \psi(x_l^*) = \Delta x\psi'(x^{**}), x^{**} \in (x_l^*, x_{l+1}^*). \tag{7}$$

The maximal length of the non-uniform mesh steps is bounded by the maximal value of $\psi'(x)$, and it exists since $\psi(x)$ is continuously differentiable. Therefore,

$$\Delta x_{l+1} \le v\Delta x, v = \max_{x\in[0,1]} |\psi'(x)|, \tag{8}$$

That is, $\max_{l=0(1)L} |\Delta x_{l+1}| \le v\Delta x$, and hence, $\|\boldsymbol{\Delta x}\|_\infty \le v\Delta x = v/(L+1) < v/L$, where $\boldsymbol{\Delta x} = [\Delta x_1, \Delta x_2, ..., \Delta x_{L+1}]$. As a result, we find that

$$\|\boldsymbol{\Delta x}\|_\infty = O(\Delta x) = O\left(\frac{1}{L}\right) \text{ and } \|\boldsymbol{\Delta x}\|_\infty \to 0 \text{ as } L \to \infty. \tag{9}$$

Similarly, we can prove that the mesh points sequences $\{y_m\}_{m=1}^{M+1}$ and $\{z_n\}_{n=1}^{N+1}$ along y- and z-directions are well defined, and the limiting value of mesh-steps diminishes for a sufficiently large value of M and N respectively. As a result, we find that the maximum mesh spacing is conversely identified with the quantity of mesh points. Britz [32] and Sundqvist et al. [33] applied such a mesh network to wind-driven ocean circulation model and digital electrochemistry. Recently, Jha et al. [34-36] obtained compact operators on quasi-variable meshes to discretize two- and three-dimensions elliptic PDEs and described third- and fourth-order accurate formulation for solving higher dimensions elliptic PDEs on a non-uniform mesh topology.

3. Compact operators and a high-order scheme

We shall refer to the numerical and exact values at the mesh-point (x_l, y_m, z_n, t_j) by $w_{l,m,n,j}$ and $W_{l,m,n,j}$ respectively. For the ADEs, we need estimates of first- and second-order spatial derivatives and first-order temporal derivatives. Compact operators with minimal stencil width will help construct all such approximations. Upon using a linear combination of solution values at six neighboring mesh points $(x_{l\pm1}, y_m, z_n, t_j), (x_l, y_{m\pm1}, z_n, t_j), (x_l, y_m, z_{n\pm1}, t_j)$ and one central mesh-point (x_l, y_m, z_n, t_j), we define

$$\mathcal{F}_x W_{l,m,n,j} = \Delta x_l \mathcal{A}(p, \Delta x_l) \begin{bmatrix} W_{l,m,n,j} \\ W_{l+1,m,n,j} \\ W_{l-1,m,n,j} \end{bmatrix}, \quad \mathcal{S}_x W_{l,m,n,j} = \Delta x_l^2 \mathcal{B}(p, \Delta x_l) \begin{bmatrix} W_{l,m,n,j} \\ W_{l+1,m,n,j} \\ W_{l-1,m,n,j} \end{bmatrix}, \tag{10}$$

$$\mathcal{F}_y W_{l,m,n,j} = \Delta y_m \mathcal{A}(q, \Delta y_m) \begin{bmatrix} W_{l,m,n,j} \\ W_{l,m+1,n,j} \\ W_{l,m-1,n,j} \end{bmatrix}, \quad \mathcal{S}_y W_{l,m,n,j} = \Delta y_m^2 \mathcal{B}(q, \Delta y_m) \begin{bmatrix} W_{l,m,n,j} \\ W_{l,m+1,n,j} \\ W_{l,m-1,n,j} \end{bmatrix}, \tag{11}$$

$$\mathcal{F}_z W_{l,m,n,j} = \Delta z_n \mathcal{A}(r, \Delta z_n) \begin{bmatrix} W_{l,m,n,j} \\ W_{l,m,n+1,j} \\ W_{l,m,n-1,j} \end{bmatrix}, \quad \mathcal{S}_z W_{l,m,n,j} = \Delta z_n^2 \mathcal{B}(r, \Delta z_n) \begin{bmatrix} W_{l,m,n,j} \\ W_{l,m,n+1,j} \\ W_{l,m,n-1,j} \end{bmatrix}, \tag{12}$$

where

$$\mathcal{A}(s,\hbar) = \left[\frac{s}{1+\hbar s} \quad \frac{1}{(1+\hbar s)(2+\hbar s)\hbar} \quad -\frac{1+\hbar s}{(2+\hbar s)\hbar}\right], \quad \mathcal{B}(s,\hbar) = \frac{2}{\hbar^2}\left[\frac{-1}{1+\hbar s} \quad \frac{1}{(\hbar s+1)(2+\hbar s)} \quad \frac{1}{\hbar s+2}\right], \tag{13}$$

and $(s,\hbar) \in \{(p,\Delta x_l), (q,\Delta y_m), (r,\Delta z_n)\}$. The utilization of Taylor's series yields

$$\begin{bmatrix} \mathcal{F}_x W_{l,m,n,j} \\ \mathcal{F}_y W_{l,m,n,j} \\ \mathcal{F}_z W_{l,m,n,j} \end{bmatrix} = \begin{bmatrix} \Delta x_l W^x_{l,m,n,j} \\ \Delta y_m W^y_{l,m,n,j} \\ \Delta z_n W^z_{l,m,n,j} \end{bmatrix} + \begin{bmatrix} O(\Delta x_l^3) \\ O(\Delta y_m^3) \\ O(\Delta z_n^3) \end{bmatrix}, \quad \begin{bmatrix} \mathcal{S}_x W_{l,m,n,j} \\ \mathcal{S}_y W_{l,m,n,j} \\ \mathcal{S}_z W_{l,m,n,j} \end{bmatrix} = \begin{bmatrix} \Delta x_l^2 W^{xx}_{l,m,n,j} \\ \Delta y_m^2 W^{yy}_{l,m,n,j} \\ \Delta z_n^2 W^{zz}_{l,m,n,j} \end{bmatrix} + \begin{bmatrix} O(\Delta x_l^4) \\ O(\Delta y_m^4) \\ O(\Delta z_n^4) \end{bmatrix}. \tag{14}$$

Therefore, at the j^{th}-time level, all the parameter-dependent commutative difference operators $\mathcal{F}_x, \mathcal{F}_y, \mathcal{F}_z$ and $\mathcal{S}_x, \mathcal{S}_y, \mathcal{S}_z$ provide second-order precise approximations to the partial derivatives of first- and second-order in spatial directions. In particular, when $p = 0$, we get $\mathcal{F}_x = \mu_x \delta_x$ and $\mathcal{S}_x = \delta_x^2$, where μ_x and δ_x are averaging and central difference operators for uniformly spaced meshes along x-space. A similar observation about the operators $\mathcal{F}_y$, $\mathcal{S}_y$ and $\mathcal{F}_z$, $\mathcal{S}_z$ can be seen with $q = 0$ and $r = 0$ in y- and z-directions, respectively. Likewise, one can receive compact operators at $(j + 1)^{\text{th}}$-time level. A straightforward compact discretization using (10)-(12) to the equation (1) yields the system of difference equations

$$\begin{aligned}&\epsilon(\Delta x_l^{-2}\mathcal{S}_x + \Delta y_m^{-2}\mathcal{S}_y + \Delta z_n^{-2}\mathcal{S}_z)W_{l,m,n,j}\\ &= G(x_l, y_m, z_n, t_j, W_{l,m,n,j}, \Delta x_l^{-1}\mathcal{F}_x W_{l,m,n,j}, \Delta y_m^{-1}\mathcal{F}_y W_{l,m,n,j}, \Delta z_n^{-1}\mathcal{F}_z W_{l,m,n,j}, \Delta t\tilde{W}^t_{l,m,n,j})\\ &\quad + O(\Delta x_l^2 + \Delta y_m^2 + \Delta z_n^2 + \Delta t),\end{aligned} \tag{15}$$

where $\tilde{W}^t_{l,m,n,j}$ is the forward-difference derivative along the temporal direction, and it is given by

$$\tilde{W}^t_{l+\alpha,m+\beta,n+\gamma,j} = \frac{1}{\Delta t}\left[W_{l+\alpha,m+\beta,n+\gamma,j+1} - W_{l+\alpha,m+\beta,n+\gamma,j}\right], \quad \alpha, \beta, \gamma \in \{0, \pm 1\}. \tag{16}$$

The seven points compact scheme (15) is only first and second-order precise along the temporal and spatial direction. Moreover, it preserves the theoretical order in both the circumstances of uniform and quasi-variable mesh spacings. Such a type of formulation is known as a supra-convergent scheme [37]. But, computationally, it results in either slow convergence or unsatisfactory solution values with a reasonably practical number of mesh points, maybe with uniform meshes ($p = q = r = 0$) or quasi-variable meshes $(p \neq 0 \vee q \neq 0 \vee r \neq 0)$. Therefore, we need to develop a new numerical technique that is higher-order accurate in spatial and temporal directions. In this way, we obtain numerical solution values with a faster rate of convergence in small computing time. To develop the high-order compact discretization to the ADEs (1), we begin with the time-dependent partial differential equations

$$\epsilon\nabla^2 W \equiv \epsilon(W^{xx} + W^{yy} + W^{zz}) = G(x, y, z, t). \tag{17}$$

At the mesh points (x_l, y_m, z_n, t_j), the equation (17) can be written as

$$\epsilon(W^{xx}_{l,m,n,j} + W^{yy}_{l,m,n,j} + W^{zz}_{l,m,n,j}) = G(x_l, y_m, z_n, t_j) \equiv G_{l,m,n,j}. \tag{18}$$

Now, let us consider the linear combination

$$\begin{aligned}\chi \equiv \chi(x_l, y_m, z_n, t_j) &= \Delta x_l^2 \Delta y_m^2 \Delta z_n^2[\sigma(p\Delta x_l^2 G^x_{l,m,n,j} + q\Delta y_m^2 G^y_{l,m,n,j} + r z_n^2 G^z_{l,m,n,j})\\ &\quad + \rho(\Delta x_l \Delta x_{l+1} G^{xx}_{l,m,n,j} + \Delta y_m \Delta y_{m+1} G^{yy}_{l,m,n,j} + \Delta z_n \Delta z_{n+1} G^{zz}_{l,m,n,j}) + G_{l,m,n,j}].\end{aligned} \tag{19}$$

Using the equations (10)-(12) and (17) in (18), we find

$$\begin{aligned}\chi \equiv \epsilon\tilde{\nabla}^2 W_{l,m,n,j} &+ \epsilon\Delta x_l^2 \Delta y_m^2 \Delta z_n^2[(\sigma - 1/3)(p\Delta x_l^2 W^{xxx}_{l,m,n,j} + q\Delta y_m^2 W^{yyy}_{l,m,n,j} + r\Delta z_n^2 W^{zzz}_{l,m,n,j})\\ &+ (\rho - 1/12)(\Delta x_l \Delta x_{l+1} W^{xxxx}_{l,m,n,j} + \Delta y_m \Delta y_{m+1} W^{yyyy}_{l,m,n,j} + \Delta z_n \Delta z_{n+1} W^{zzzz}_{l,m,n,j})] + HOT,\end{aligned} \tag{20}$$

where, the higher-order term $HOT = \Delta x_l^2 \Delta y_m^2 \Delta z_n^2 O(\Delta x_l^2 + \Delta y_m^2 + \Delta z_n^2)^2$ and

$$\begin{aligned}\tilde{\nabla}^2 \equiv\ & (\Delta y_m^2 \Delta z_n^2 \mathcal{S}_x + \Delta x_l^2 \Delta z_n^2 \mathcal{S}_y + \Delta x_l^2 \Delta y_m^2 \mathcal{S}_z) \\ & + \rho(\Delta x_{l+1} \Delta x_l + \Delta y_{m+1} \Delta y_m) \Delta z_n^2 \mathcal{S}_x \mathcal{S}_y + \sigma \Delta y_m^2 \Delta z_n^2 (q \Delta y_m \mathcal{F}_y + r \Delta z_n \mathcal{F}_z) \mathcal{S}_x \\ & + \rho(\Delta z_{n+1} \Delta z_n + \Delta y_{m+1} \Delta y_m) \Delta x_l^2 \mathcal{S}_y \mathcal{S}_z + \sigma \Delta z_n^2 \Delta x_l^2 (r \Delta z_n \mathcal{F}_z + p \Delta x_l \mathcal{F}_x) \mathcal{S}_y \\ & + \rho(\Delta z_{n+1} \Delta z_n + \Delta x_{l+1} \Delta x_l) \Delta y_m^2 \mathcal{S}_x \mathcal{S}_z + \sigma \Delta x_l^2 \Delta y_m^2 (p \Delta x_l \mathcal{F}_x + q \Delta y_m \mathcal{F}_y) \mathcal{S}_z, \end{aligned} \tag{21}$$

is the high-order finite-difference discretization of Laplacian operator $\nabla^2 = \partial_{xx}^2 + \partial_{yy}^2 + \partial_{zz}^2$. Note that the coefficient of $W_{l,m,n,j}^{xxx}, W_{l,m,n,j}^{xxxx}$ etc. in the equation (20) vanishes for the free parameter value $\sigma = 1/3,\ \rho = 1/12$ and consequently, the equation (20) results in

$$\chi \equiv \epsilon \tilde{\nabla}^2 W_{l,m,n,j} + HOT. \tag{22}$$

Furthermore, utilizing the compact operators (10)-(12) in the linear combination (19) and (22) yields seven-point high-order discretization as

$$\epsilon \tilde{\nabla}^2 W_{l,m,n,j} = \Delta x_l^2 \Delta y_m^2 \Delta z_n^2 \sum_{(\alpha,\beta,\gamma) \in S_1} \theta_{l+\alpha,m+\beta,n+\gamma} G_{l+\alpha,m+\beta,n+\gamma,j} + HOT, \tag{23}$$

where

$$\begin{gathered} G_{l+\alpha,m+\beta,n+\gamma,j} = G(x_{l+\alpha}, y_{m+\beta}, z_{n+\gamma}, t_j), \\ \theta_{l\pm1,m,n} = \frac{1}{96}\phi_{\pm}(p, \Delta x_l), \quad \theta_{l,m\pm1,n} = \frac{1}{96}\phi_{\pm}(q, \Delta y_m), \quad \theta_{l,m,n\pm1} = \frac{1}{96}\phi_{\pm}(r, \Delta z_n), \\ \theta_{l,m,n} = -\frac{1}{6}[\phi_0(p, \Delta x_l) + \phi_0(q, \Delta y_m) + \phi_0(r, \Delta z_n)], \\ \phi_+(s,h) = 8 + sh(12 - 22sh + 22s^2h^2), \quad \phi_-(s,h) = 8 - sh(12 + 10sh - 5s^2h^2), \\ \phi_0(s,h) = 2s^2h^2(sh-1) - 1, \quad (s,h) \in \{(p, \Delta x_l), (q, \Delta y_m), (r, \Delta z_n)\}. \end{gathered}$$

and summation in (23) runs over the set $S_1 = \{(0,0,0), (\pm1,0,0), (0,\pm1,0), (0,0,\pm1)\}$.

Since the linear combination (19) is multiplied with $\Delta x_l^2 \Delta y_m^2 \Delta z_n^2$, therefore in either case of quasi-variable meshes or evenly distributed meshes, the magnitude of truncation error (*TE*) remains the same, and it is given by

$$TE = HOT / [\Delta x_l^2 \Delta y_m^2 \Delta z_n^2] = O(\Delta x_l^2 + \Delta y_m^2 + \Delta z_n^2)^2. \tag{24}$$

Thus, the compact scheme (23) yields fourth-order accurate numerical solutions to the three-dimensional time-dependent PDE (17) provided $\Delta x_l \approx \Delta y_m \approx \Delta z_n$.

Now, we shall extend high-order discretization (23) to the mildly nonlinear ADEs (1), containing the unknown *W*(*x, y, z, t*) and its partial first-order derivatives in temporal and spatial directions as nonlinear terms. We implement two-level in time and begin with the weighted average of solution values at the current and immediate next temporal level in the following manner:

$$\hat{W}_{l+\alpha,m+\beta,n+\gamma,j} = \eta W_{l+\alpha,m+\beta,n+\gamma,j+1} + (1-\eta) W_{l+\alpha,m+\beta,n+\gamma,j},\ 0 \le \eta \le 1. \tag{25}$$

Consider the following approximations

$$\tilde{W}_{l,m+\beta,n+\gamma,j}^{x} = \mathcal{A}(p, \Delta x_l) \begin{bmatrix} \hat{W}_{l,m+\beta,n+\gamma,j} \\ \hat{W}_{l+1,m+\beta,n+\gamma,j} \\ \hat{W}_{l-1,m+\beta,n+\gamma,j} \end{bmatrix}, (\beta,\gamma) \in S_2, \tag{26}$$

$$\tilde{W}^{y}_{l+\alpha,m,n+\gamma,j} = \mathcal{A}(q,\Delta y_m)\begin{bmatrix} \hat{W}_{l+\alpha,m,n+\gamma,j} \\ \hat{W}_{l+\alpha,m+1,n+\gamma,j} \\ \hat{W}_{l+\alpha,m-1,n+\gamma,j} \end{bmatrix}, (\alpha,\gamma) \in S_2, \tag{27}$$

$$\tilde{W}^{z}_{l+\alpha,m+\beta,n,j} = \mathcal{A}(r,\Delta z_n)\begin{bmatrix} \hat{W}_{l+\alpha,m+\beta,n,j} \\ \hat{W}_{l+\alpha,m+\beta,n+1,j} \\ \hat{W}_{l+\alpha,m+\beta,n-1,j} \end{bmatrix}, (\alpha,\beta) \in S_2, \tag{28}$$

$$\tilde{W}^{xx}_{l,m+\beta,n+\gamma,j} = \mathcal{B}(p,\Delta x_l)\begin{bmatrix} \hat{W}_{l,m+\beta,n+\gamma,j} \\ \hat{W}_{l+1,m+\beta,n+\gamma,j} \\ \hat{W}_{l-1,m+\beta,n+\gamma,j} \end{bmatrix}, (\beta,\gamma) \in S_2, \tag{29}$$

$$\tilde{W}^{yy}_{l+\alpha,m,n+\gamma,j} = \mathcal{B}(q,\Delta y_m)\begin{bmatrix} \hat{W}_{l+\alpha,m,n+\gamma,j} \\ \hat{W}_{l+\alpha,m+1,n+\gamma,j} \\ \hat{W}_{l+\alpha,m-1,n+\gamma,j} \end{bmatrix}, (\alpha,\gamma) \in S_2, \tag{30}$$

$$\tilde{W}^{zz}_{l+\alpha,m+\beta,n,j} = \mathcal{B}(r,\Delta z_n)\begin{bmatrix} \hat{W}_{l+\alpha,m+\beta,n,j} \\ \hat{W}_{l+\alpha,m+\beta,n+1,j} \\ \hat{W}_{l+\alpha,m+\beta,n-1,j} \end{bmatrix}, (\alpha,\beta) \in S_2, \tag{31}$$

$$\begin{bmatrix} \tilde{W}^{x}_{l-1,m,n,j} \\ \tilde{W}^{x}_{l+1,m,n,j} \end{bmatrix} = \mathcal{C}(p,\Delta x_l)\begin{bmatrix} \hat{W}_{l,m,n,j} \\ \hat{W}_{l+1,m,n,j} \\ \hat{W}_{l-1,m,n,j} \end{bmatrix}, \tag{32}$$

$$\begin{bmatrix} \tilde{W}^{y}_{l,m-1,n,j} \\ \tilde{W}^{y}_{l,m+1,n,j} \end{bmatrix} = \mathcal{C}(q,\Delta y_m)\begin{bmatrix} \hat{W}_{l,m,n,j} \\ \hat{W}_{l,m+1,n,j} \\ \hat{W}_{l,m-1,n,j} \end{bmatrix}, \tag{33}$$

$$\begin{bmatrix} \tilde{W}^{z}_{l,m,n-1,j} \\ \tilde{W}^{z}_{l,m,n+1,j} \end{bmatrix} = \mathcal{C}(r,\Delta z_n)\begin{bmatrix} \hat{W}_{l,m,n,j} \\ \hat{W}_{l,m,n+1,j} \\ \hat{W}_{l,m,n-1,j} \end{bmatrix}, \tag{34}$$

where $s_2 = \{(0,\pm 1),(\pm 1,0)\}$ and

$$\mathcal{C}(s,h)=\begin{bmatrix} \frac{2+sh}{(1+sh)h} & \frac{-1}{(1+sh)(2+sh)h} & -\frac{3+sh}{(2+sh)h} \\ -\frac{2+sh}{1+sh} & \frac{3+2sh}{(1+sh)(2+sh)h} & \frac{1+sh}{(2+sh)h} \end{bmatrix}, (s,h)\in\{(p,\Delta x_l),(q,\Delta y_m),(r,\Delta z_n)\}.$$

For $(\alpha,\beta,\gamma)\in S_1\sim\{(0,0,0)\}$, we consider the following functional approximations

$$\tilde{G}_{l+\alpha,m+\beta,n+\gamma,j}=G(x_{l+\alpha},y_{m+\beta},z_{n+\gamma},\tilde{t}_j,\hat{W}_{l+\alpha,m+\beta,n+\gamma,j},\tilde{W}^x_{l+\alpha,m+\beta,n+\gamma,j},\tilde{W}^y_{l+\alpha,m+\beta,n+\gamma,j},\tilde{W}^z_{l+\alpha,m+\beta,n+\gamma,j},\tilde{W}^t_{l+\alpha,m+\beta,n+\gamma,j}), \quad (35)$$

where $\tilde{t}_j=\eta t_j+(1-\eta)t_{j+1}$ is the convex combination of two neighboring mesh-point along with time level. The additional first-order partial derivatives regarding linear combinations of functional values and approximated derivative values are

$$\hat{W}^x_{l,m,n,j}=\tilde{W}^x_{l,m,n,j}+\sigma_x\Delta x_l[\tilde{G}_{l+1,m,n,j}-\tilde{G}_{l-1,m,n,j}-\epsilon(\tilde{W}^{yy}_{l+1,m,n,j}-\tilde{W}^{yy}_{l-1,m,n,j}+\tilde{W}^{zz}_{l+1,m,n,j}-\tilde{W}^{zz}_{l-1,m,n,j})], \quad (36)$$

$$\hat{W}^y_{l,m,n,j}=\tilde{W}^y_{l,m,n,j}+\sigma_y\Delta y_m[\tilde{G}_{l,m+1,n,j}-\tilde{G}_{l,m-1,n,j}-\epsilon(\tilde{W}^{xx}_{l,m+1,n,j}-\tilde{W}^{xx}_{l,m-1,n,j}+\tilde{W}^{zz}_{l,m+1,n,j}-\tilde{W}^{zz}_{l,m-1,n,j})], \quad (37)$$

$$\hat{W}^z_{l,m,n,j}=\tilde{W}^z_{l,m,n,j}+\sigma_z\Delta z_n[\tilde{G}_{l,m,n+1,j}-\tilde{G}_{l,m,n-1,j}-\epsilon(\tilde{W}^{xx}_{l,m,n+1,j}-\tilde{W}^{xx}_{l,m,n-1,j}+\tilde{W}^{yy}_{l,m,n+1,j}-\tilde{W}^{yy}_{l,m,n-1,j})], \quad (38)$$

where $\sigma_x,\sigma_y,\sigma_z$ and η are free parameters to be driven in so as to obtain an error-reduced accurate scheme. The functional approximation at the central mesh-point of j^{th}-time level is defined as

$$\tilde{G}_{l,m,n,j}=G(x_l,y_m,z_n,\tilde{t}_j,\tilde{W}_{l,m,n,j},\hat{W}^x_{l,m,n,j},\hat{W}^y_{l,m,n,j},\hat{W}^z_{l,m,n,j},\tilde{W}^t_{l,m,n,j}). \quad (39)$$

Then, for the following values of free parameters

$$\sigma_x=-\frac{1+p\Delta x_l}{6\epsilon(2+p\Delta x_l)},\quad \sigma_y=-\frac{1+q\Delta y_m}{6\epsilon(2+q\Delta y_m)},\quad \sigma_z=-\frac{1+r\Delta z_m}{6\epsilon(2+r\Delta z_m)},\quad \eta=\frac{1}{2} \quad (40)$$

the modified difference relation

$$\epsilon\tilde{\nabla}^2W_{l,m,n,j}=\Delta x_l^2\Delta y_m^2\Delta z_n^2\sum_{(\alpha,\beta,\gamma)\in S_1}\theta_{l+\alpha,m+\beta,n+\gamma}\tilde{G}_{l+\alpha,m+\beta,n+\gamma,j}, \quad (41)$$

is $O(\Delta x_l^2\Delta y_m^2\Delta z_n^2\{(\Delta x_l^2+\Delta y_m^2+\Delta z_n^2)\Delta t+\Delta t^2\})$-accurate and therefore, for the temporal step-size $\Delta t\propto\Delta x_l^2\approx\Delta y_m^2\approx\Delta z_n^2$, the scheme (41) provides fourth-order accurate solution values on the quasi-variable mesh topology. We observed that the new scheme's theoretical order (41) remains unchanged even if uniform mesh steps are considered. For the computer implementation of the numerical scheme (41), we shall use the Newton-Raphson method for nonlinear problems and the ADI method for linear equations, as described in the subsequent section.

4. ADE and ADI method

We consider discretization of the three space dimensions unsteady ADE

$$\epsilon\nabla^2W=W^t+bW^x+cW^y+dW^z+f(x,y,z,t), \quad (42)$$

where b,c and d are constants and $W(x, y, z, t)$ is the concentration of mass transfer [10, 13]. The initial and boundary values associated with (42) are the same as defined in (2)-(5). The application of the compact scheme (41) to the linear ADE (42) in terms of compact operator form results in

$$\chi_L W_{l,m,n,j+1} = \chi_R W_{l,m,n,j} + \Sigma_{RHS}, \tag{43}$$

where

$$\begin{aligned}\chi_L = 1 &+ P_1\mathcal{F}_x + P_2\mathcal{S}_x + P_3\mathcal{F}_y + P_4\mathcal{S}_y + P_5\mathcal{F}_z + P_6\mathcal{S}_z + P_7\mathcal{S}_x\mathcal{F}_y + P_8\mathcal{S}_x\mathcal{F}_z + P_9\mathcal{F}_x\mathcal{S}_y + P_{10}\mathcal{S}_y\mathcal{F}_z + P_{11}\mathcal{F}_x\mathcal{S}_z + P_{12}\mathcal{F}_y\mathcal{S}_z \\ &+ P_{13}\mathcal{S}_x\mathcal{S}_y + P_{14}\mathcal{S}_x\mathcal{S}_z + P_{15}\mathcal{S}_y\mathcal{S}_z + P_{16}\mathcal{F}_x\mathcal{F}_y + P_{17}\mathcal{F}_y\mathcal{F}_z + P_{18}\mathcal{F}_x\mathcal{F}_z,\end{aligned} \tag{44}$$

$$\begin{aligned}\chi_R = 1 &+ Q_1\mathcal{F}_x + Q_2\mathcal{S}_x + Q_3\mathcal{F}_y + Q_4\mathcal{S}_y + Q_5\mathcal{F}_z + Q_6\mathcal{S}_z + Q_7\mathcal{S}_x\mathcal{F}_y + Q_8\mathcal{S}_x\mathcal{F}_z + Q_9\mathcal{F}_x\mathcal{S}_y + Q_{10}\mathcal{S}_y\mathcal{F}_z + Q_{11}\mathcal{F}_x\mathcal{S}_z \\ &+ Q_{12}\mathcal{F}_y\mathcal{S}_z + Q_{13}\mathcal{S}_x\mathcal{S}_y + Q_{14}\mathcal{S}_x\mathcal{S}_z + Q_{15}\mathcal{S}_y\mathcal{S}_z + Q_{16}\mathcal{F}_x\mathcal{F}_y + Q_{17}\mathcal{F}_y\mathcal{F}_z + Q_{18}\mathcal{F}_x\mathcal{F}_z,\end{aligned} \tag{45}$$

$$\Sigma_{RHS} = \sum_{(\alpha,\beta,\gamma)\in S} R_{l+\alpha,m+\beta,n+\gamma} f_{l+\alpha,m+\beta,n+\gamma,j}, f_{l+\alpha,m+\beta,n+\gamma,j} = f(x_{l+\alpha}, y_{m+\beta}, z_{n+\gamma}, \tilde{t}_j),$$

and expressions of $R_{\alpha,\beta,\gamma}, (\alpha,\beta,\gamma) \in S_1, P_i, Q_i, i = 1(1)18,$ are presented in Appendix A. The compact operator form (43) is obtained by expressing the solution values regarding compact operators and their composites, except at the central mesh-point (x_l, y_m, z_n, t_j). For example, the operator equations (10) give us

$$W_{l+1,m,n,j} = \frac{1}{2}[2 + (1 + p\Delta x_l)\{(1 + p\Delta x_l)\mathcal{S}_x + 2\mathcal{F}_x\}]W_{l,m,n,j}, \tag{46}$$

and

$$W_{l-1,m,n,j} = \frac{1}{2}[2 + \mathcal{S}_x - 2\mathcal{F}_x]W_{l,m,n,j}. \tag{47}$$

Similarly, all the remaining solution values except $W_{l,m,n,j}$ and $W_{l,m,n,j+1}$ at j^{th} and $(j+1)^{\text{th}}$-time level respectively, can be obtained in terms of compact operators and their composites.

The system of equations (43) results in a large sparse high bandwidth matrix, and solving such a matrix system is cumbersome due to exceptionally high computing time and memory. Thus, we rewrite the system (43) in a memory-efficient and factored form.

Let

$$\tilde{\chi}_L = (1 + P_1\mathcal{F}_x + P_2\mathcal{S}_x)(1 + P_3\mathcal{F}_y + P_4\mathcal{S}_y)(1 + P_5\mathcal{F}_z + P_6\mathcal{S}_z), \tag{48}$$

$$\tilde{\chi}_R = (1 + Q_1\mathcal{F}_x + Q_2\mathcal{S}_x)(1 + Q_3\mathcal{F}_y + Q_4\mathcal{S}_y)(1 + Q_5\mathcal{F}_z + Q_6\mathcal{S}_z). \tag{49}$$

Then, from (44), (45), (48) and (49), we find that

$$(\tilde{\chi}_L - \chi_L)W_{l,m,n,j+1} = \chi^+ W_{l,m,n,j+1}, \tag{50}$$

$$(\tilde{\chi}_R - \chi_R)W_{l,m,n,j} = \chi^- W_{l,m,n,j}, \tag{51}$$

where

$$\begin{aligned}\chi^\pm = &E_1^\pm\mathcal{F}_x\mathcal{F}_y + E_2^\pm\mathcal{F}_x\mathcal{F}_z + E_3^\pm\mathcal{F}_y\mathcal{F}_z + E_4^\pm\mathcal{S}_x\mathcal{S}_y + E_5^\pm\mathcal{S}_x\mathcal{S}_y\mathcal{S}_z + E_6^\pm\mathcal{S}_x\mathcal{S}_y\mathcal{F}_z + E_7^\pm\mathcal{S}_x\mathcal{S}_z + E_8^\pm\mathcal{S}_x\mathcal{F}_y + E_9^\pm\mathcal{S}_x\mathcal{F}_y\mathcal{S}_z \\ &+ E_{10}^\pm\mathcal{S}_x\mathcal{F}_y\mathcal{F}_z + E_{11}^\pm\mathcal{S}_x\mathcal{F}_z + E_{12}^\pm\mathcal{S}_y\mathcal{S}_z + E_{13}^\pm\mathcal{S}_y\mathcal{F}_z + E_{14}^\pm\mathcal{F}_x\mathcal{S}_y + E_{15}^\pm\mathcal{F}_x\mathcal{S}_y\mathcal{S}_z + E_{16}^\pm\mathcal{F}_x\mathcal{S}_y\mathcal{F}_z + E_{17}^\pm\mathcal{F}_x\mathcal{S}_z \\ &+ E_{18}^\pm\mathcal{F}_x\mathcal{F}_y\mathcal{S}_z + E_{19}^\pm\mathcal{F}_x\mathcal{F}_y\mathcal{F}_z + E_{20}^\pm\mathcal{F}_y\mathcal{S}_z,\end{aligned}$$

and

$$E_1^+ = P_1P_3 - P_{16}, E_2^+ = P_1P_5 - P_{18}, E_3^+ = P_3P_5 - P_{17}, E_4^+ = P_2P_4 - P_{13}, E_5^+ = P_2P_4P_6, E_6^+ = P_2P_4P_5, E_7^+ = P_2P_6 - P_{14},$$
$$E_8^+ = P_2P_3 - P_7, E_9^+ = P_2P_3P_6, E_{10}^+ = P_2P_3P_5, E_{11}^+ = P_2P_5 - P_8, E_{12}^+ = P_4P_6 - P_{15}, E_{13}^+ = P_4P_5 - P_{10}, \ E_{14}^+ = P_1P_4 - P_9,$$
$$E_{15}^+ = P_1P_4P_6, E_{16}^+ = P_1P_4P_5, E_{17}^+ = P_1P_6 - P_{11}, E_{18}^+ = P_1P_3P_6, E_{19}^+ = P_1P_3P_5, E_{20}^+ = P_3P_6 - P_{12}.$$

The expression for E_i^- is obtained from E_i^+ by symbolic replacement of P to Q. As a result, the discrete relation (43) can be expressed in the following manner

$$\tilde{\chi}_L W_{l,m,n,j+1} = \tilde{\chi}_R W_{l,m,n,j} + \chi^+ W_{l,m,n,j+1} + \chi^- W_{l,m,n,j} + \sum_{RHS}. \tag{52}$$

Upon simplifying all of $E_i^{\pm}, i = 1(1)20,$ using multi-dimensions Taylor's expansion and using the relation $W_{l,m,n,j+1} = W_{l,m,n,j} + O(\Delta t),$ we obtain

$$\chi^+ W_{l,m,n,j+1} + \chi^- W_{l,m,n,j} = O(\Delta t(\Delta x_l^2 + \Delta y_m^2 + \Delta z_n^2)^2). \tag{53}$$

Consequently, the scheme (52) further simplifies the compact operator splitting scheme

$$\tilde{\chi}_L W_{l,m,n,j+1} = \tilde{\chi}_R W_{l,m,n,j} + \sum_{RHS}. \tag{54}$$

The scheme (54) solves the ADE (42) with the same magnitude of truncation error obtained in the scheme (41). Now, it is easy to write (54) as an ADI form in the following manner:

$$(1 + P_5\mathcal{F}_z + P_6\mathcal{S}_z)W_{l,m,n}^{**} = \sum_{RHS}, \quad n = 1, ..., N, \tag{55}$$

$$(1 + P_3\mathcal{F}_y + P_4\mathcal{S}_y)W_{l,m,n}^{*} = W_{l,m,n}^{**}, \quad m = 1, ..., M, \tag{56}$$

$$(1 + P_1\mathcal{F}_x + P_2\mathcal{S}_x)W_{l,m,n,j+1} = W_{l,m,n}^{*}, \quad l = 1, ..., L, \ j = 0, 1, 2, ... \tag{57}$$

where $W_{l,m,n}^{*}$ and $W_{l,m,n}^{**}$ are the intermediate step values between j^{th} and $(j + 1)^{\text{th}}$-time levels. For computation purposes, the intermediate step boundary values needed for sweeping may be obtained in the following ways.

With the available values of $W_{l,m,n,j}$ for the fixed time level j, we solve the tri-diagonal system of equations (55), and it demands the boundary data $W_{l,m,n}$ at $n = 0$ and $n = N + 1$. These intermediate boundary data are determined from (56) and (57) in the following manner:

Upon using the boundary data (2)-(5) and the scheme (57), it provides the first intermediate boundary value as

$$W_{l,m,n}^{*} = (1 + P_1\mathcal{F}_x + P_2\mathcal{S}_x)W_{l,m,n,j+1}, \begin{cases} l = 1(1)L, m = 0, M+1, n = 0(1)N+1, \\ l = 1(1)L, m = 0(1)M+1, n = 0, N+1, \end{cases} \tag{58}$$

Next, with the help of (58), the second boundary data can be determined from (56) as

$$W_{l,m,n}^{**} = (1 + P_3\mathcal{F}_y + P_4\mathcal{S}_y)W_{l,m,n}^{*}, l = 1, ..., L, m = 1, ..., M, n = 0, N+1. \tag{59}$$

Therefore, the boundary data (59) along with the tri-diagonal system (55) yields the intermediate values $W_{l,m,n}^{**}$, and then, the boundary data (58) along with the tri-diagonal system (56) may be solved for $W_{l,m,n}^{*}$. Finally, the prescribed boundary data (2)-(5) and the tri-diagonal system (57) can be computed to obtain the solution value $W_{l,m,n,j+1}$ at the next time level.

5. Coupled Burger's equation and stability analysis

The nonlinear analytic solution of one space dimension Burger's equation, appearing in the weak non-stationary shock wave and turbulence model, was proposed by Cole [38]. Subsequently, [39, 40] reported solutions to the 2D Burger's equation. The three-dimensional coupled Burger's equations were discussed in recent years in [41, 42]. The equations are

$$\epsilon(\psi^{xx}+\psi^{yy}+\psi^{zz})=\psi^{t}+U\psi^{x}+V\psi^{y}+W\psi^{z}, \tag{60}$$

where $\psi\equiv\psi(x,y,z,t)=[U,V,W]$ is the irrotational velocity vector and $R_e=1/\epsilon$ is the Reynolds number used to predict patterns of fluid flow.

The numerical scheme (41) can be extended to the coupled equation (60) by substituting $\psi=U,V,W$ in the approximations (16) and (25)-(34). The further formulations are obtained as

$$\tilde{G}^{(\psi)}_{l+\alpha,m+\beta,n+\gamma,j}=\tilde{\psi}^{t}_{l+\alpha,m+\beta,n+\gamma,j}+\tilde{U}_{l+\alpha,m+\beta,n+\gamma,j}\tilde{\psi}^{x}_{l+\alpha,m+\beta,n+\gamma,j}+\tilde{V}_{l+\alpha,m+\beta,n+\gamma,j}\tilde{\psi}^{y}_{l+\alpha,m+\beta,n+\gamma,j}+\tilde{W}_{l+\alpha,m+\beta,n+\gamma,j}\tilde{\psi}^{z}_{l+\alpha,m+\beta,n+\gamma,j}, \tag{61}$$

where $\psi=U,V,W.$ The additional first-order partial derivatives approximations (36)-(38) can be extended as

$$\hat{\psi}^{x}_{l,m,n,j}=\tilde{\psi}^{x}_{l,m,n,j}+\sigma_x\Delta x_l[\tilde{G}^{(U)}_{l+1,m,n,j}-\tilde{G}^{(U)}_{l-1,m,n,j}-\epsilon(\tilde{\psi}^{yy}_{l+1,m,n,j}-\tilde{\psi}^{yy}_{l-1,m,n,j}+\tilde{\psi}^{zz}_{l+1,m,n,j}-\tilde{\psi}^{zz}_{l-1,m,n,j})], \tag{62}$$

$$\hat{\psi}^{y}_{l,m,n,j}=\tilde{\psi}^{y}_{l,m,n,j}+\sigma_y\Delta y_m[\tilde{G}^{(V)}_{l,m+1,n,j}-\tilde{G}^{(V)}_{l,m-1,n,j}-\epsilon(\tilde{\psi}^{xx}_{l,m+1,n,j}-\tilde{\psi}^{xx}_{l,m-1,n,j}+\tilde{\psi}^{zz}_{l,m+1,n,j}-\tilde{\psi}^{zz}_{l,m-1,n,j})], \tag{63}$$

$$\hat{\psi}^{z}_{l,m,n,j}=\tilde{\psi}^{z}_{l,m,n,j}+\sigma_z\Delta z_n[\tilde{G}^{(W)}_{l,m,n+1,j}-\tilde{G}^{(W)}_{l,m,n-1,j}-\epsilon(\tilde{\psi}^{xx}_{l,m,n+1,j}-\tilde{\psi}^{xx}_{l,m,n-1,j}+\tilde{\psi}^{yy}_{l,m,n+1,j}-\tilde{\psi}^{yy}_{l,m,n-1,j})], \tag{64}$$

where values of σ_x, σ_y and σz are same as defined in (40) and $\psi=U,V,W.$ Then, the high-order quasi-variable mesh discretization to the coupled equation (60) is given by the system of difference relations

$$T^{(U)}\equiv\epsilon\tilde{\nabla}^2U_{l,m,n,j}-\sum_{(\alpha,\beta,\gamma)\in S_1}\theta_{l+\alpha,m+\beta,n+\gamma}\tilde{G}^{(U)}_{l+\alpha,m+\beta,n+\gamma,j}=0, \tag{65}$$

$$T^{(V)}\equiv\epsilon\tilde{\nabla}^2V_{l,m,n,j}-\sum_{(\alpha,\beta,\gamma)\in S_1}\theta_{l+\alpha,m+\beta,n+\gamma}\tilde{G}^{(V)}_{l+\alpha,m+\beta,n+\gamma,j}=0, \tag{66}$$

$$T^{(W)}\equiv\epsilon\tilde{\nabla}^2W_{l,m,n,j}-\sum_{(\alpha,\beta,\gamma)\in S_1}\theta_{l+\alpha,m+\beta,n+\gamma}\tilde{G}^{(W)}_{l+\alpha,m+\beta,n+\gamma,j}=0. \tag{67}$$

The solution data to the next time level for the system of nonlinear difference relations (65)-(67) is obtained by applying the Newton-Raphson method

$$\begin{bmatrix}U_{l,m,n,j+1}\\V_{l,m,n,j+1}\\W_{l,m,n,j+1}\end{bmatrix}=\begin{bmatrix}U_{l,m,n,j}\\V_{l,m,n,j}\\W_{l,m,n,j}\end{bmatrix}-\mathcal{J}^{-1}\begin{bmatrix}T^{(U)}\\T^{(V)}\\T^{(W)}\end{bmatrix}, \tag{68}$$

where

$$\mathcal{J} = \begin{bmatrix} \partial T^{(U)}/\partial U_{l,m,n,j} & \partial T^{(U)}/\partial V_{l,m,n,j} & \partial T^{(U)}/\partial W_{l,m,n,j} \\ \partial T^{(V)}/\partial U_{l,m,n,j} & \partial T^{(V)}/\partial V_{l,m,n,j} & \partial T^{(V)}/\partial W_{l,m,n,j} \\ \partial T^{(W)}/\partial U_{l,m,n,j} & \partial T^{(W)}/\partial V_{I,m,n,j} & \partial T^{(W)}/\partial W_{l,m,n,j} \end{bmatrix},$$

is the Jacobian matrix. With the iteration scheme (68), we will compare the error and behavior of the quasi-variable compact scheme's numerical solutions with a uniform mesh high-order scheme.

Next, we shall describe the Hopf-Cole transformation to the coupled equation (60), which is equivalent to the coupled equation

$$\epsilon(U^{xx} + U^{yy} + U^{zz}) = U^t + UU^x + VU^y + WU^z, \tag{69}$$

$$\epsilon(V^{xx} + V^{yy} + V^{zz}) = V^t + UV^x + VV^y + WV^z, \tag{70}$$

$$\epsilon(W^{xx} + W^{yy} + W^{zz}) = W^t + UW^x + VW^y + WW^z. \tag{71}$$

Let $\psi = \nabla g,$ then $U = \partial_x g, V = \partial_y g$ and $W = \partial_z g.$ Therefore, equations (69)-(71), upon integrating with respect to *x*, *y* and *z* respectively, result in the following form

$$\epsilon(g^{xx} + g^{yy} + g^{zz}) = g^t + \frac{1}{2}[(g^x)^2 + (g^y)^2 + (g^z)^2] + \rho(t). \tag{72}$$

Again, using the substitution $g = -2\epsilon \ln(H(x, y, z, t))$, equation (72) reduces to

$$\epsilon(H^{xx} + H^{yy} + H^{zz}) = H^t + \frac{1}{2\epsilon}\rho(t)H. \tag{73}$$

Finally, the transformation $H(x, y, z, t) = \phi(x, y, z, t) \exp\left(\frac{1}{2\epsilon}\int \rho(t)dt\right)$ to the equation (73) results in a standard diffusion equation

$$\epsilon(\phi^{xx} + \phi^{yy} + \phi^{zz}) = \phi^t. \tag{74}$$

We shall describe the Fourier stability of the ADI compact scheme to the standard diffusion equation (74). One can obtain the high-order accurate ADI scheme of (74) upon replacing W to ϕ and substituting $b = c = d = 0, f(x, y, z, t) = 0$, in the scheme (54). Following the technique discussed in [27, 31], we take $\varepsilon^j_{l,m,n} = \xi^j e^{i(\alpha x_l + \beta y_m + \gamma z_n)}$, as the error at j^{th}-time level, where ξ is an amplification factor, a complex constant, α, β, γ are real numbers and $i = \sqrt{-1}$. Then, from the equation (54), the error equation is given by

$$\begin{aligned}&(1 + P_1\mathcal{F}_x + P_2\mathcal{S}_x)(1 + P_3\mathcal{F}_y + P_4\mathcal{S}_y)(1 + P_5\mathcal{F}_z + P_6\mathcal{S}_z)\varepsilon^{j+1}_{l,m,n} \\ &= (1 + Q_1\mathcal{F}_x + Q_2\mathcal{S}_x)(1 + Q_3\mathcal{F}_y + Q_4\mathcal{S}_y)(1 + Q_5\mathcal{F}_z + Q_6\mathcal{S}_z)\varepsilon^j_{l,m,n}.\end{aligned} \tag{75}$$

Since $\varepsilon^{j+1}_{l,m,n} = \xi\varepsilon^j_{l,m,n}$, $(x_{l-1}, y_{m-1}, z_{n-1}) = (x_l, y_m, z_n) - (\Delta x_l, \Delta y_m, \Delta z_n)$ and $(x_{l+1}, y_{m+1}, z_{n+1}) = (x_l, y_m, z_n) + (\Delta x_{l+1}, \Delta y_{m+1}, \Delta z_{n+1})$. Therefore, from (10)-(12), we find that $\mathcal{S}_x\varepsilon^{j+1}_{l,m,n} = \xi\mathcal{S}_x\varepsilon^j_{l,m,n}$ and $\mathcal{F}_x\varepsilon^{j+1}_{l,m,n} = \xi\mathcal{F}_x\varepsilon^j_{l,m,n}$. Thus, the value of amplification factor is obtained as $\xi = \xi_x\xi_y\xi_z$, where

$$\xi_x = \frac{N_x}{D_x} = \frac{1 + Q_1\mathcal{F}_x + Q_2\mathcal{S}_x}{1 + P_1\mathcal{F}_x + P_2\mathcal{S}_x}, \quad \xi_y = \frac{N_y}{D_y} = \frac{1 + Q_3\mathcal{F}_y + Q_4\mathcal{S}_y}{1 + P_3\mathcal{F}_y + P_4\mathcal{S}_y} \text{ and } \xi_z = \frac{N_z}{D_z} = \frac{1 + Q_5\mathcal{F}_z + Q_6\mathcal{S}_z}{1 + P_5\mathcal{F}_z + P_6\mathcal{S}_z}. \tag{76}$$

If we denote $L_x = \frac{N_x - D_x}{N_x + D_x}, L_y = \frac{N_y - D_y}{N_y + D_y}, L_z = \frac{N_z - D_z}{N_z + D_z},$ then, one can express $\xi_x = \frac{1+L_x}{1-L_x}$ and $L_x = \frac{A_x + iB_x}{C_x + iD_x},$ where

$$\begin{aligned}
A_x &= 2\epsilon\Delta t[\{\cos(\alpha\,\Delta x_{l+1}) - 1\} - (p\Delta x_l + 1)\{1 - \cos(\alpha\,\Delta x_l)\}]/[(2 + p\Delta x_l)\Delta x_l \Delta x_{l+1}],\\
B_x &= 2\epsilon\Delta t[\sin(\alpha\,\Delta x_{l+1}) - (1 + p\Delta x_l)\sin(\alpha\,\Delta x_l)]/[(2 + p\Delta x_l)\Delta x_l \Delta x_{l+1}],\\
C_x &= (27p^4\Delta x_l^4 + 48p\Delta x_l + 16)\cos(\alpha\,\Delta x_{l+1})/[48(1 + p\Delta x_l)(2 + p\Delta x_l)]\\
&\quad - (27p^4\Delta x_l^4 + 32p\Delta x_l - 16)(1 + p\Delta x_l)\cos(\alpha\,\Delta x_l)/[48(p\Delta x_l + 2)]\\
&\quad + (27p^5\Delta x_l^5 + 32p^2\Delta x_l^2 + 80p\Delta x_l + 80)/[48(p\Delta x_l + 1)],\\
D_x &= (p\Delta x_l + 1)(27p^4\Delta x_l^4 + 32p\Delta x_l - 16)\sin(p\,\Delta x_l)/[48(2 + p\Delta x_l)]\\
&\quad + (27p^4\Delta x_l^4 + 48p\Delta x_l + 16)\sin(\Delta x_{l+1}p)/[48(\Delta x_l p + 1)(2 + \Delta x_l p)].
\end{aligned}$$

Upon simplification, one finds that

$$\begin{aligned}
A_xC_x + B_xD_x &= -\epsilon\Delta t s_1 \sin^2(\alpha\,\Delta x_l/2)/[12(p\Delta x_l + 2)\Delta x_l\,\Delta x_{l+1}] - \epsilon\Delta t s_2 \sin^2(\alpha\,\Delta x_{l+1}/2)/[12(p\Delta x_l + 2)\Delta x_{l+1}^2]\\
&\quad + \epsilon\Delta t(3p\Delta x_l + 2)s_3 \sin^2(\alpha\,\{\Delta x_l + \Delta x_{l+1}\}/2)/[12(p\Delta x_l + 2)^2\Delta x_l\Delta x_{l+1}],
\end{aligned} \tag{77}$$

where

$$\begin{aligned}
s_1 &= 57p^5\Delta x_l^5 + 27p^4\Delta x_l^4 + 64p^2\Delta x_l^2 + 96p\Delta x_l + 64,\\
s_2 &= 27p^5\Delta x_l^5 + 27(1 - p^4\Delta x_l^4) + 32p^2\Delta x_l^2 + 32p\Delta x_l + 37,\\
s_3 &= 9p^4\Delta x_l^4 - 6p^3\Delta x_l^3 + 4p^2\Delta x_l^2 + 8p\Delta x_l - 16.
\end{aligned}$$

Since $\epsilon > 0, 0 < \Delta x_l, \Delta y_m, \Delta z_n < 1,$ and $0 < p, q, r < 1,$ we observe that $s_1 > 0$, $s_2 > 0$ and $s_3 < 3p^3\Delta x_l^3 + 4p^2\Delta x_l^2 + 8p\Delta x_l - 16 < 7p^2\Delta x_l^2 + 8p\Delta x_l - 1.$ That is, $s_3 < 15p^2\Delta x_l^2 - 16 < 15 - 16 = -1 < 0,$ and hence, $A_xC_x + B_xD_x < 0.$ As a result, we obtain $|\xi_x| < 1.$ In the same manner, we can establish that $|\xi_y| < 1$ and $|\xi_z| < 1.$ Consequently, $|\xi| \le 1,$ which proves the unconditional stability of the high-order quasi-variable meshes two-level implicit compact scheme applied to transformed coupled Burger's equation in (3 + 1)-dimensions.

6. Numerical experiments and error estimation

This section is devoted to simulations executed on the Navier-Stokes equations, Burger's equations, and ADEs. We executed computer programming in C, and symbolic computations in Maple on Mac operating system. We shall examine linear problems to illustrate the effectiveness of the new quasi-variable meshes alternating direction implicit scheme of high-order accuracy. To solve a difference equation's nonlinear system, we have used the Newton-Raphson method [43, 44], and the iterations continue until the absolute error tolerance reaches 10^{-10}. The initial and time-dependent boundary data in each problem are determined from the analytic solution values on the cuboid's surface. In each case, the time domain is taken as $0 \le t \le 1$, and error in the solution values are computed at $t = 1$. In the following numerical simulations, all the spatial directions have the same quantity of mesh points ($L = M = N$). The number of mesh points in the temporal direction is determined from $\Delta t = \lambda/(LM) \approx \lambda\Delta x_l \Delta y_m, \lambda = 1.6,$ and $J = \left\lceil \frac{1}{\Delta t} \right\rceil,$ where $\lceil \circ \rceil$ the ceiling function computes the least integer value greater than or equal to $1/\Delta t.$ We shall determine maximum absolute errors and corresponding numerical order as a measure of accuracies using the following formula

$$\ell_\infty^{(L,M,N)} = \max_{\substack{l=1(1)L, m=1(1)M \\ n=1(1)N, j=1(1)J}} \left| W_{l,m,n,j} - w_{l,m,n,j} \right|, \qquad \Theta_\infty = \log_2 \left[\frac{\ell_\infty^{(L,M,N)}}{\ell_\infty^{(2L,2M,2N)}} \right]. \tag{78}$$

In the following experiments, we shall investigate the proposed scheme's advantage over existing uniform mesh high-order implicit compact schemes.

Example 6.1 We consider the source less heat equation in the three-dimensions

$$\epsilon(W^{xx} + W^{yy} + W^{zz}) = W^{t}, \; 0 < x, y, z < 1, \; t > 0. \tag{79}$$

It administers quiescent medium thermal incident and temperature distribution in solid with constant thermal diffusivity [45]. It also appears in an unsteady mass transfer process with fixed diffusion. The model possesses an analytic solution $W(x, y, z, t) = e^{-3\epsilon\pi^2 t} \sin(\pi x)\sin(\pi y)\sin(\pi z)$, where ϵ is the coefficient of dispersion (diffusion) [46]. The numerical simulations with $\epsilon \ll 1$ show that solution values preserve order and accuracy in case of uniform meshes scheme. However, at a large diffusion coefficient value, the stream tends to be dominated by laminar heat flow. Therefore, for $\epsilon \gg 1$, we need to observe the behaviour of solution values. The order and accuracies deteriorated while taking uniform meshes, and thus, we have considered quasi-variable meshes in a high-order implicit scheme to capture the maximum absolute error and computational order for $\epsilon = 10^0, 10^1$ and 10^2 at the final time t = 1 in Table 1. Figure 1 shows the sliced three-dimensional view of the temperature profile $W(x, y, z, t)$ in the *xy*-, *yz*-, *zx*-plane evaluated at z = 0.2, x = 0.8, and y = 0.8 respectively with ϵ = 10 and L = 4 at the time level t = 1.

Table 1. The ℓ_∞-norm errors and numerical order in Example 6.1

L	J	p	q	r	$\ell_\infty^{(L,M,N)}$	Θ_∞
$\epsilon = 10^0$						
4	10	0.60	0.70	0.40	6.30*e*-05	---
8	40	0.30	0.20	0.40	3.47*e*-06	4.2
16	160	0.10	0.10	0.06	1.18*e*-07	4.9
$\epsilon = 10^1$						
4	10	0.40	0.70	0.72	5.74*e*-05	---
8	40	0.30	0.20	0.24	3.45*e*-06	4.1
16	160	0.10	0.10	0.11	1.39*e*-07	4.6
$\epsilon = 10^2$						
4	10	0.74	0.74	0.74	7.66*e*-04	---
8	40	0.20	0.20	0.10	4.67*e*-05	4.0
16	160	0.10	0.10	0.06	2.43*e*-06	4.3

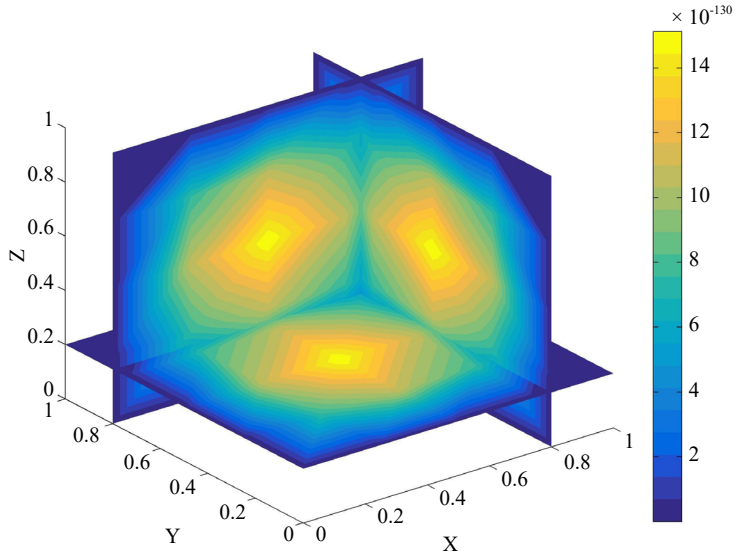

Figure 1. Sliced three-dimensional view of temperature profile in Example 6.1

Example 6.2 The three-dimensional ADE

$$\epsilon(W^{xx}+W^{yy}+W^{zz})=W^{t}+bW^{x}+cW^{y}+dW^{z},\ 0<x,y,z<1,\ t>0. \tag{80}$$

possesses the concentration of mass transfer $W(x,y,z,t)$ in the analytic form

$$W(x,y,z,t)=\frac{1}{(4t+1)^{3/2}}\exp\left[-\frac{(x-bt-0.5)^2+(y-ct-0.5)^2+(z-dt-0.5)^2}{\epsilon(4t+1)}\right].$$

The accuracy in numerical solutions is obtained for the various diffusion and advection coefficient values. In the following experiments, we shall take $b = c = d$. Table 2 and Table 3 represents the solution errors at $\epsilon=10^{-3},10^{-4},\ b=0,\ (b<\epsilon<1),$ using the uniform and quasi-variable meshes compact formulation, respectively. Table 4 shows the solution error at $\epsilon=10^{-4},10^{-5},10^{-6},\ b$ = 1.0, $(b<\epsilon=1),$ using quasi-variable meshes compact scheme. Table 5 represents the solution error for the various possibilities of diffusion and advection coefficients: $\epsilon=10^{-2},\ b$ = 2.0, $(\epsilon<b, b>1);$ $\epsilon=10^{-2},\ b$ = 0.8, $(\epsilon<b<1);$ $\epsilon=10^{-2}, b$ = 10^{-2}, $(\epsilon=b<1)$ and $\epsilon=10^{-2},\ b$ = 10^{-3}, $(b<\epsilon<1)$. A uniform meshes high-order compact scheme ($p = q = r = 0$) fails to obtain the solution values in all the above cases accurately. In contrast, a non-uniformly spaced quasi-variable meshes optimum, accurate implicit compact scheme determines the solution values precisely, and the same reflects in tabulated maximum absolute errors and computational orders. In Table 6, the ℓ_∞-errors using the proposed method at L = 20, $\epsilon=10^{-2}$ shows superiority over the existing method [7]. Figure 2 shows the sliced three-dimensional surface plot of the concentration of mass transfer W (x, y, z, t) in the xy-, yz-, zx-plane evaluated at z = 0.2, x = 0.8, and y = 0.8 respectively with ϵ = 0.01, $b = c = d$ = 0.01 and L = 8 at the time level t =1.

Table 2. The ℓ_∞-norm errors and numerical order in Example 6.2

L	J	$\ell_\infty^{(L,M,N)}$	Θ_∞	$\ell_\infty^{(L,M,N)}$	Θ_∞	$\ell_\infty^{(L,M,N)}$
		$\epsilon = 10^{-3}$	$\epsilon = 10^{-3}$	$\epsilon = 10^{-4}$	$\epsilon = 10^{-4}$	$\epsilon = 10^{-5}$
4	10	7.91*e*-01	---	8.98*e*-01	---	9.09*e*-01
8	40	5.23*e*-01	0.6	8.60*e*-01	0.06	9.05*e*-01
16	160	1.08*e*-01	2.3	7.27*e*-01	0.24	8.90*e*-01
32	640	1.46*e*-03	6.2	3.78*e*-01	0.94	8.23*e*-01

Table 3. The ℓ_∞-norm errors and numerical order in Example 6.2

L	J	p	q	r	$\ell_\infty^{(L,M,N)}$	Θ_∞
$\epsilon = 10^{-3}$						
4	10	0.10	0.10	0.3100	9.99*e*-04	---
8	40	0.18	0.18	0.2300	8.52*e*-05	3.6
16	160	0.01	0.09	0.0800	5.78*e*-06	3.9
32	640	0.01	0.01	0.0383	3.15*e*-07	4.2
$\epsilon = 10^{-4}$						
4	10	0.46	0.41	0.4100	9.77*e*-03	---
8	40	0.10	0.04	0.1600	6.06*e*-04	4.0
16	160	0.00	0.03	0.0861	3.92*e*-05	4.0
32	640	0.01	0.01	0.0375	2.09*e*-06	4.2

Table 4. The ℓ_∞-norm errors and numerical order in Example 6.2

L	J	p	q	r	$\ell_\infty^{(L,M,N)}$	Θ_∞
$\epsilon = 10^{-4}$						
4	10	0.300	0.300	0.900	9.36*e*-02	---
8	40	0.300	0.020	0.300	5.25*e*-03	4.2
16	160	0.100	0.080	0.040	3.00*e*-04	4.1
32	640	0.030	0.030	0.030	1.51*e*-05	4.3
$\epsilon = 10^{-5}$						
4	10	0.900	0.010	0.700	9.17*e*-02	---
8	40	0.800	0.500	0.300	5.92*e*-03	4.0
16	160	0.100	0.100	0.100	3.65*e*-04	4.0
32	640	0.035	0.036	0.037	2.11*e*-05	4.1
$\epsilon = 10^{-6}$						
4	10	0.900	0.010	0.700	9.24*e*-02	---
8	40	0.450	0.300	0.300	5.63*e*-03	4.0
16	160	0.110	0.100	0.100	3.47*e*-04	4.0
32	640	0.036	0.036	0.036	2.86*e*-05	3.6

Table 5. The ℓ_∞-norm errors and numerical order in Example 6.2 with $\epsilon = 10^{-2}$

L	J	p	q	r	$\ell_\infty^{(L,M,N)}$	Θ_∞
$b = 2.0$						
4	10	0.800	0.80	0.80	6.50*e*-06	---
8	40	0.400	0.30	0.86	4.03*e*-07	4.0
16	160	0.100	0.10	0.11	2.36*e*-08	4.1
32	640	0.038	0.04	0.04	9.84*e*-10	4.6
$b = 0.8$						
4	10	0.6000	0.1	0.1	9.08*e*-04	---
8	40	0.2000	0.1	0	5.52*e*-05	4.0
16	160	0.0100	0.1	0	3.60*e*-06	3.9
32	640	0.0001	0	0	2.57*e*-07	3.8
$b = 10^{-2}$						
4	10	0.0	0.0	0.280	5.25*e*-02	---
8	40	0.0	0.0	0.286	3.09*e*-03	4.2
16	160	0.0	0.0	0.0	1.73*e*-04	4.2
32	640	0.0	0.0	0.0	1.03*e*-05	4.1
$b = 10^{-3}$						
4	10	0.0	0.0	0.280	5.78*e*-02	---
8	40	0.0	0.0	0.286	3.61*e*-03	4.0
16	160	0.0	0.0	0.0	1.72*e*-04	4.4
32	640	0.0	0.0	0.0	1.03*e*-05	4.1

Table 6. Comparison of ℓ_∞-norm errors in Example 6.2 with $L = 20$, $\epsilon = 10^{-2}$

b	T	p	q	r	$\ell_\infty^{(L,M,N)}$	ℓ_∞-error in [7]
0.80	0.05	0	0	0.10	1.68*e*-08	5.82*e*-04
2.00	0.05	0	0	0.10	1.63*e*-06	7.76*e*-04
0.80	0.20	0	0	0.10	5.40*e*-04	7.72*e*-04
2.00	0.20	0.05	0.05	0.05	2.54*e*-02	1.76*e*-01

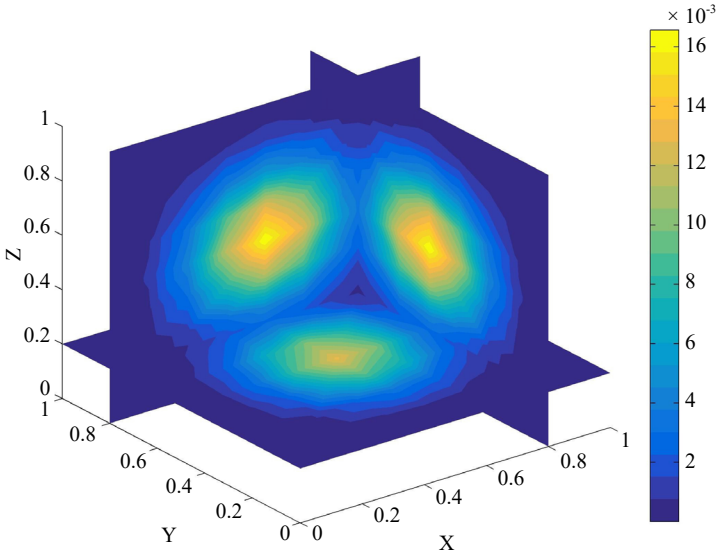

Figure 2. Sliced three-dimensional view of mass transfer in Example 6.2

Example 6.3 Consider the transient nonlinear convection-diffusion equation

$$\epsilon(W^{xx}+W^{yy}+W^{zz})=W^{t}+W(W^{x}+W^{y}+W^{z}),\ 0<x,y,z<1,\ t>0, \tag{81}$$

where $W(x,y,z,t)$ represents the velocity field in x, y, z-directions and ϵ is the kinematic viscosity [47]. It possesses analytic solutions

$$W(x,y,z,t)=\exp[\{\alpha x+\beta y-(\alpha+\beta)z+2(\alpha^2+\alpha\beta+\beta^2)t\}/\epsilon]. \tag{82}$$

Comparing the analytic solution (82) and approximate numerical solution values at the time level $t = 1$ and parameter value $\alpha=\beta=0.8, \epsilon=1,$ with quasi-variable meshes and uniformly spaced mesh points in Table 7, it is evident that ℓ_∞-norm errors and convergence order using quasi-variable mesh points high-order compact scheme is better than the uniform meshes high-order scheme.

Example 6.4 In the computational experiments of Burger's equation (60), we will take the analytic solution [41, 42],

$$U(x,y,z,t)=-2A\pi\epsilon\beta\gamma e^{-\mu\epsilon t}\cos(A\pi x)\sin(B\pi y)\sin(C\pi z), \tag{83a}$$

$$V(x,y,z,t)=-2B\pi\epsilon\beta\gamma e^{-\mu\epsilon t}\sin(A\pi x)\cos(B\pi y)\sin(C\pi z), \tag{83b}$$

$$W(x,y,z,t)=-2C\pi\epsilon\beta\gamma e^{-\mu\epsilon t}\sin(A\pi x)\sin(B\pi y)\cos(C\pi z), \tag{83c}$$

where $\gamma=[\alpha+\beta e^{-\mu\epsilon t}\sin(A\pi x)\sin(B\pi y)\sin(C\pi z)]^{-1}$ and $\mu=\pi^2(A^2+B^2+C^2)$. The wavenumbers are set at $A = B = C = 3$. The amplitude controlling parameters are taken as $\alpha = 1.0$. The cubic domain is non-uniformly partitioned with 4, 8 and 16 mesh points along each spatial directions. The ℓ_∞-errors of the U-velocity at the Reynolds number $R_e=1/\epsilon=10^2, 10^3$ and time level $t = 1$ with quasi-variable meshes high-resolution implicit compact scheme are given in Table 8 and Table 9 at $\beta = 0.1$ and 1.0, respectively. Change in the Reynolds number and amplitude parameter value produces slight variations in the magnitude of ℓ_∞-errors. Simulations with $p = q = r = 0$ results in ill-behaved solution values and oscillating computational order. Figures 3 to 5 show the sliced three-dimensional view of the velocity vector

$U(x, y, z, t)$, $V(x, y, z, t)$ and $W(x, y, z, t)$ respectively in the xy-, yz-, zx-plane evaluated at $z = 0.1$, $x = 0.8$, and $y = 0.9$ respectively with the Reynolds number value $R_e = 102$, wavenumbers $A = B = C = 3$, amplitude controlling parameters $\alpha = \beta = 1.0$ and $L = 16$ at the time level $t = 1$.

Table 7. The ℓ_∞-norm errors and numerical order in Example 6.3

L	J	p	q	r	$\ell_\infty^{(L,M,N)}$	Θ_∞
4	10	0	0	0	9.41*e*-01	---
8	40	0	0	0	2.11*e*-01	2.2
16	160	0	0	0	2.56*e*-02	3.0
4	10	0.1100	0.0100	0.0200	9.38*e*-02	---
8	40	0.0120	0.0170	0.0100	7.65*e*-03	3.6
16	160	0.0029	0.0033	0.0026	5.54*e*-04	3.8

Table 8. The ℓ_∞-norm errors and numerical order in Example 6.4 with $\beta = 0.1$

L	J	p	q	r	$\ell_\infty^{(L,M,N)}$	Θ_∞
$\epsilon = 10^{-2}$						
4	10	0.500	0.300	0.500	4.64e-03	---
8	40	0.010	0.130	0.110	2.73e-04	4.1
16	160	0.001	0.002	0.001	1.66e-05	4.0
$\epsilon = 10^{-3}$						
4	10	0.600	0.5	0.5	3.63e-04	---
8	40	0.200	0	0	2.75e-05	3.7
16	160	0.010	0	0	1.65e-06	4.1

Table 9. The ℓ_∞-norm errors and numerical order in Example 6.4 with $\beta = 1.0$

L	J	p	q	r	$\ell_\infty^{(L,M,N)}$	Θ_∞
$\epsilon = 10^{-2}$						
4	10	0.700	0.800	0.790	8.15*e*-03	---
8	40	0.200	0.400	0.300	5.06*e*-04	4.0
16	160	0.001	0.100	0.111	3.03*e*-05	4.1
$\epsilon = 10^{-3}$						
4	10	0.200	0.300	0.500	7.14*e*-04	---
8	40	0.100	0.300	0.350	4.75*e*-05	4.0
16	160	0.010	0.110	0.10	1.89*e*-06	4.7

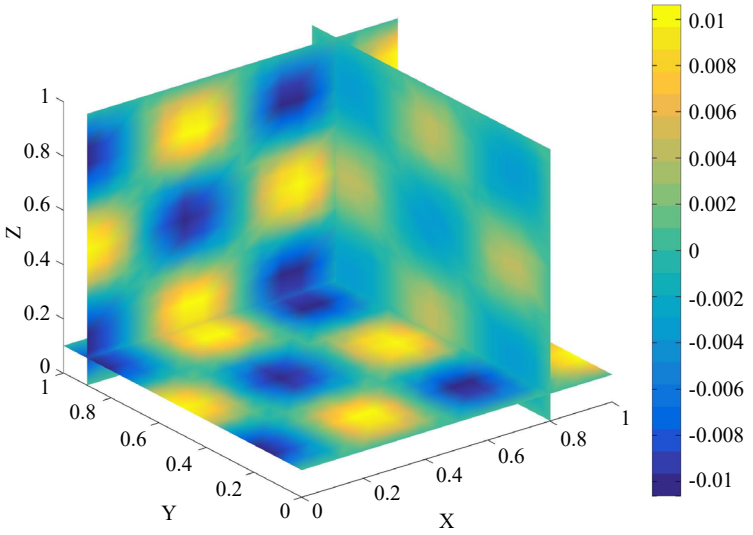

Figure 3. Sliced three-dimensional view of velocity $U(x, y, z, t)$ in Example 6.4

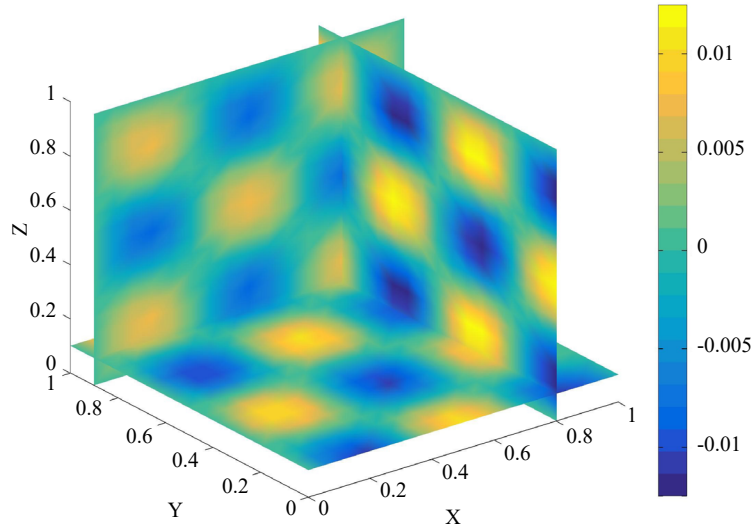

Figure 4. Sliced three-dimensional view of velocity $V(x, y, z, t)$ in Example 6.4

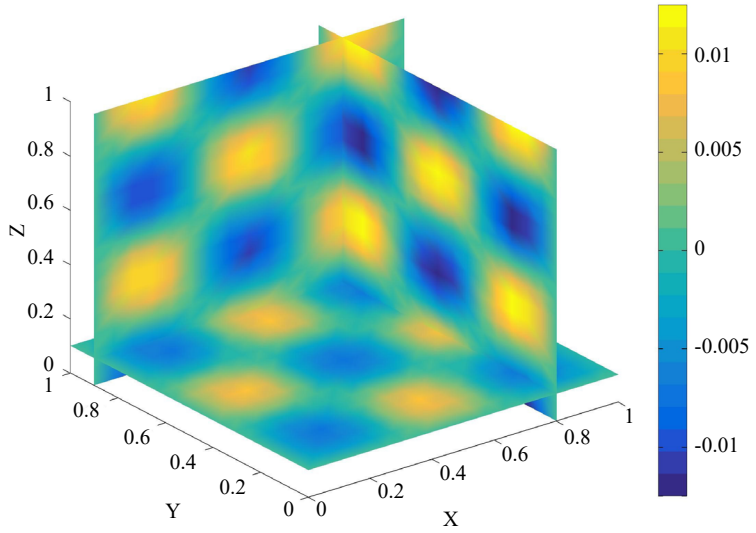

Figure 5. Sliced three-dimensional view of velocity $W(x, y, z, t)$ in Example 6.4

Example 6.5 The time-dependent three space dimensions incompressible Navier-Stokes equations in the non-dimensional form is given by

$$\epsilon(U^{xx} + U^{yy} + U^{zz}) = U^t + UU^x + VU^y + WU^z + \wp^x, \tag{84a}$$

$$\epsilon(V^{xx} + V^{yy} + V^{zz}) = V^t + UV^x + VV^y + WV^z + \wp^y, \tag{84b}$$

$$\epsilon(W^{xx} + W^{yy} + W^{zz}) = W^t + UW^x + VW^y + WW^z + \wp^z, \tag{84c}$$

where (U, V, W) is the velocity vector, $\wp = \wp(x, y, z, t) = (U^2 + V^2 + W^2)/2$, is the pressure, and Reynolds number $R_e = 1/\epsilon$, is used to predict patterns of fluid flow [48, 49]. In the numerical simulations with Navier-Stokes equations, the number of mesh points of the computational domain with each side length being a unity is chosen as 4, 8, and 16 to compute the numerical convergence rate. The analytic solution for computing ℓ_∞-errors are taken as

$$U(x, y, z, t) = -\beta e^{-\epsilon\alpha^2 t}[e^{\beta x}\sin(\alpha z + \beta y) + e^{\beta z}\cos(\alpha y + \beta x)], \tag{85a}$$

$$V(x, y, z, t) = -\beta e^{-\epsilon\alpha^2 t}[e^{\beta y}\sin(\alpha x + \beta z) + e^{\beta x}\cos(\alpha z + \beta y)], \tag{85b}$$

$$W(x, y, z, t) = -\beta e^{-\epsilon\alpha^2 t}[e^{\beta z}\sin(\alpha y + \beta x) + e^{\beta y}\cos(\alpha x + \beta z)], \tag{85c}$$

where α, β are constants and it controls the frequency and amplitude of the solution values. The value of the Reynolds number is assumed to 10 and 100, other data are set at $\alpha = 2\pi$ and $\beta = 0.1$. The uniform meshes' ℓ_∞-norm errors are discouraging. Therefore, numerical results pertaining to quasi-variable meshes compact scheme for computing ℓ_∞-errors in numerical and exact pressure are recorded in Table 10. By increasing the value of the Reynolds number from 10 to 100 and decreasing the controlling parameter value β from 0.1 to 0.01, the computational order remains unchanged in the uniform and non-uniform distribution of mesh points. Figure 6 shows the sliced three-dimensional view of numerical pressure $\wp(x, y, z, t)$ on a 16 × 16 × 16 cell discretization along the cross sections $(x, y, z) = (0.8, 0.8, 0.2)$ with the Reynolds number value $R_e = 10$ and parameter value $\alpha = 2\pi$, $\beta = 0.1$ at the time level $t = 1$.

Table 10. The ℓ_∞-norm errors and numerical order in Example 6.5 with $\beta = 0.1$

L	J	p	q	r	$\ell_\infty^{(L,M,N)}$	Θ_∞
$\epsilon = 10^{-1}$						
4	10	0.720	0	0	9.05e-05	---
8	40	0.090	0	0	5.66e-06	4.0
16	160	0.010	0	0	3.57e-07	4.0
$\epsilon = 10^{-2}$						
4	10	0.970	0.99	0.99	3.42e-02	---
8	40	0.180	0	0	3.98e-03	3.1
16	160	0.001	0	0	2.62e-04	3.9

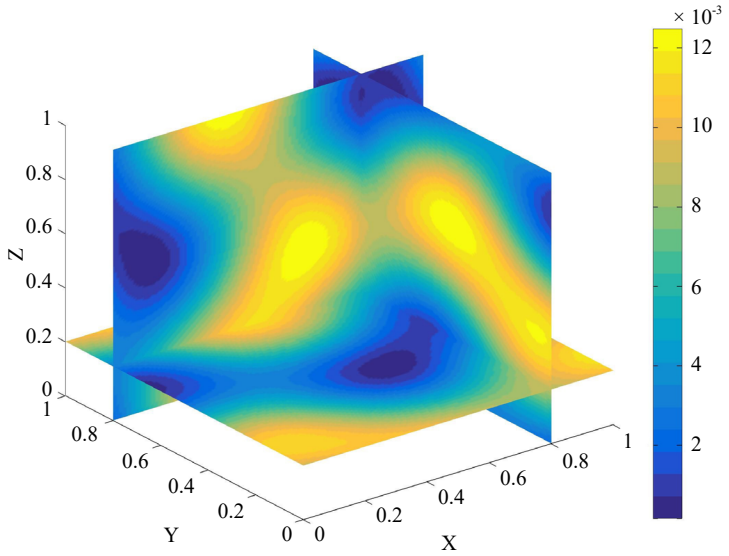

Figure 6. Sliced three-dimensional view of numerical pressure in Example 6.5

7. Conclusion

The present work described a two-level, high-resolution implicit compact scheme on a quasi-variable mesh topology for solving three-dimensional second-order linear and mildly nonlinear ADEs. The new unconditional stable scheme is derived so that the accuracy of order two in time and four in spatial direction remains unchanged on a uniformly or non-uniformly distributed mesh network. However, considering non-uniformly propagated mesh points yields more accurate solution values, as shown in the computational illustrations, which is the main highlight of the present work. Moreover, all the operators involve only three mesh points in every spatial direction; thus, presenting the numerical scheme for linear ADEs in the tri-diagonal decomposition is easy. The Thomas algorithm can solve an operator-splitting scheme with a considerably short CPU time. Moreover, the present high-order scheme needs significantly fewer mesh points to accurately resolve linear convection-dominated equations, nonlinear coupled Burger's equations, and Navier-Stokes equations in three dimensions. Numerical simulations demonstrate superior efficiency and accuracy over existing uniform mesh high-order schemes.

Acknowledgment

The Royal Society of Edinburgh, Scotland and Indian National Science Academy, India support the present research work under the international collaboration program awarded to N. Jha (No. IA/RSE/2018/129:11-04-2018).

Conflict of interest

The authors declare that they have no known competing financial interests or personal relationships that could have appeared to influence the work presented in this research paper.

References

[1] Szymkiewicz R. *Numerical Modelling in Open Channel Hydraulics*. Water Science and Technology Library. Netherland: Springer; 2010.

[2] Zlatev Z, Berkowicz R, Prahm LP. Implementation of a variable step-size variable formula in the time-integration part of a code for treatment of long-range transport of air pollutants. *Journal of Computational Physics*. 1984; 55(2): 278–301. Available from: doi: 10.1016/0021-9991(84)90007-X.

[3] Hundsdorfer WH, Verwer JG, Hundsdorfer WH. *Numerical solution of time-dependent advection-diffusion-reaction equations*. Berlin: Springer; 2003. Available from: doi: 10.1007/978-3-662-09017-6.

[4] Jiang X, Lai CH. *Numerical techniques for direct and large-eddy simulations*. Boca Raton: CRC Press; 2016. Available from: doi: 10.1201/9781420075793.

[5] Samarskii AA, Matus PP, Vabishchevich PN. *Difference schemes with operator factors*. Dordrecht: Springer; 2002. Available from: doi: 10.1007/978-94-015-9874-3_3.

[6] Saul'yev VK. *Integration of equations of parabolic type by the method of nets.* Amsterdam: Elsevier; 2014.

[7] Appadu AR, Djoko JK, Gidey HH. Performance of some finite difference methods for a 3D advection-diffusion equation. *RACSAM*. 2018; 112(4): 1179-1210. Available from: doi: 10.1007/s13398-017-0414-7.

[8] Chen H, Min C, Gibou F. A supra-convergent finite difference scheme for the Poisson and heat equations on irregular domains and non-graded adaptive Cartesian grids. *Journal of Scientific Computing*. 2007; 31(1): 19-60. Available from: doi: 10.1007/s10915-006-9122-8.

[9] Dehghan M. Numerical solution of the three-dimensional advection-diffusion equation. *Applied Mathematics and Computation*. 2004; 150(1): 5-19. Available from: doi: 10.1016/S0096-3003(03)00193-0.

[10] Ge Y, Tian ZF, Zhang J. An exponential high-order compact ADI method for 3D unsteady convection-diffusion problems. *Numerical Methods for Partial Differential Equations*. 2013; 29(1): 186-205. Available from: doi: 10.1002/num.21705.

[11] Flores E, Calvillo I. Numerical solution of 3D non-stationary heat conduction problems using the finite point-set method. *International Journal of Heat and Mass Transfer*. 2015; 87: 104-110. Available from: doi: 10.1016/j.ijheatmasstransfer.2015.03.084.

[12] Karaa S, Othman M. Two-level compact implicit schemes for three-dimensional parabolic problems. *Computers & Mathematics with Applications*. 2009; 58(2): 257-263. Available from: doi: 10.1016/j.camwa.2009.02.036.

[13] Mohanty RK, Setia N. A new high accuracy two-level implicit off-step discretization for the system of three space dimensional quasi-linear parabolic partial differential equations. *Computers & Mathematics with Applications*. 2015; 69(10): 1096-1113. Available from: doi: 10.1016/j.camwa.2015.03.004

[14] Dai W. A compact local one-dimensional scheme for solving a 3D N-carrier system with Neumann boundary conditions. *Numerical Methods for Partial Differential Equations*. 2010; 26(5): 1079-1098. Available from: doi: 10.1002/num.20476.

[15] Liao W. A high-order ADI finite difference scheme for a 3D reaction-diffusion equation with Neumann boundary condition. *Numerical Methods for Partial Differential Equations*. 2013; 29(3): 778-798. Available from: doi: 10.1002/num.21726

[16] Mohanty RK, Kumar D, Jain MK. Single-cell discretization of $O(kh^2+h^4)$ for $\partial u/\partial n$ for three-space dimensional mildly quasi-linear parabolic equation. *Numerical Methods for Partial Differential Equations*. 2003; 19(3): 327-342. Available from: doi: 10.1002/num.10050.

[17] Rubbab Q, Nazeer M, Ahmad F, Chu YM, Khan M, Kadry S. Numerical simulation of advection-diffusion equation with caputo-fabrizio time fractional derivative in cylindrical domains: Applications of pseudo-spectral collocation method. *Alexandria Engineering Journal*. 2021; 60(1): 1731-1738. Available from: doi: 10.1016/j.aej.2020.11.022.
[18] Chu YM, Shah NA, Agarwal P, Chung JD. Analysis of fractional multi-dimensional Navier–Stokes equation. *Advances in Difference Equations*. 2021; 2021(1): 1-18. Available from: doi: 10.1186/s13662-021-03250-x.
[19] Inc M, Partohaghighi M, Akinlar MA, Agarwal P, Chu YM. New solutions of fractional-order Burger-Huxley equation. *Results in Physics*. 2020; 18: 103290. Available from: doi: 10.1016/j.rinp.2020.103290.
[20] Akter S, Hafez MG, Chu YM, Hossain MD. Analytic wave solutions of beta space fractional Burgers equation to study the interactions of multi-shocks in thin viscoelastic tube filled. *Alexandria Engineering Journal*. 2021; 60(1): 877-887. Available from: doi: 10.1016/j.aej.2020.10.016.
[21] Chu YM, Shah NA, Ahmad H, Chung JD, Khaled SM. A comparative study of semi-analytical methods for solving fractional-order cauchy reaction-diffusion equation. *Fractals*. 2021; 29(6): 2150143. Available from: doi: 10.1142/S0218348X21501437.
[22] Chu YM, Rafiq N, Shams M, Akram S, Mir NA, Kalsoom H. Computer methodologies for the comparison of some efficient derivative free simultaneous iterative methods for finding roots of non-linear equations. *Computers, Materials & Continua*. 2021; 66(1): 275-290. Available from: doi: 10.32604/cmc.2020.011907.
[23] Ahmad H, Khan TA, Stanimirović PS, Chu YM, Ahmad I. Modified variational iteration algorithm-II: convergence and applications to diffusion models. *Complexity*. 2020; 8841718: 1-14. Available from: doi: 10.1155/2020/8841718.
[24] Chu YM, Bani Hani EH, El-Zahar ER, Ebaid A, Shah NA. Combination of Shehu decomposition and variational iteration transform methods for solving fractional third order dispersive partial differential equations. *Numerical Methods for Partial Differential Equations*. 2021; 1-18. Available from: doi: 10.1002/num.22755.
[25] Chu Y, Khan MI, Rehman MIU, Kadry S, Qayyum S, Waqas M. Stability analysis and modeling for the three-dimensional Darcy-Forchheimer stagnation point nanofluid flow towards a moving surface. *Applied Mathematics and Mechanics*. 2021; 42(3): 357-370. Available from: doi: 10.1007/s10483-021-2700-7.
[26] Hosseini K, Sadri K, Mirzazadeh M, Ahmadian A, Chu YM, Salahshour S. Reliable methods to look for analytical and numerical solutions of a nonlinear differential equation arising in heat transfer with the conformable derivative. *Mathematical Methods in the Applied Sciences*. 2021; 1-13. Available from: doi: 10.1002/mma.7582.
[27] Liu J, Pope GA, Sepehrnoori K. A high-resolution finite-difference scheme for non-uniform grids. *Applied Mathematical Modelling*. 1995; 19(3): 162-172. Available from: doi: 10.1016/0307-904X(94)00020-7.
[28] Manteuffel TA, White AB. The numerical solution of second-order boundary value problems on non-uniform meshes. *Mathematics of Computation*. 1986; 47(176): 511-535. Available from: doi: 10.1090/S0025-5718-1986-0856700-3.
[29] Khodier AM. A finite difference scheme on nonuniform grids. *International Journal of Computer Mathematics*. 2001; 77(1): 145-52. Available from: doi: 10.1080/00207160108805057.
[30] Bieniasz LK. A set of compact finite-difference approximations to first and second derivative. related to the extended Numerov method of Chawla on non-uniform grids. *Computing*. 2007; 81(1): 77-89. Available from: doi: 10.1007/s00607-007-0239-x.
[31] Ferziger JH, Peric M, Street RL. *Computational methods for fluid dynamics*. Berlin; Springer-Verlag; 2002. Available from: doi: 10.1007/978-3-319-99693-6.
[32] Britz D. *Digital simulation in electrochemistry*. Berlin: Springer; 2005. Available from: doi: 10.1007/978-3-319-30292-8.
[33] Sundqvist H, Veronis G. A simple finite-difference grid with non-constant intervals. *Tellus*, 1970; 22(1): 26-31. Available from: doi: 10.1111/j.2153-3490.1970.tb01933.x.
[34] Jha N, Bieniasz L. A fifth(six) order accurate, three-point compact finite difference scheme for the numerical solution of sixth order boundary value problems on geometric meshes. *Journal of Scientific Computing*. 2015; 64(3): 898-913. Available from: doi: 10.1007/s10915-014-9947-5.
[35] Jha N, Kumar N. A fourth-order accurate quasi-variable mesh compact finite-difference scheme for two-space dimensional convection-diffusion problems. *Advances in Difference Equations*. 2017; 64: 1-13. Available from: doi: 10.1186/s13662-017-1115-4.
[36] Jha N, Gopal V, Singh B. A family of compact finite difference formulations for three-space dimensional nonlinear Poisson's equations in Cartesian coordinates. *Differential Equations and Dynamical Systems*. 2018; 26(1): 105-123. Available from: doi: 10.1007/s12591-016-0314-x.
[37] Kreiss H, Manteuffel T. Supra-convergent schemes on irregular grids. *Mathematics of Computation*. 1986; 47(176): 537-554. Available from: doi: 10.1090/S0025-5718-1986-0856701-5.

[38] Cole J. On a quasi-linear parabolic equation occurring in aerodynamics. *Quarterly of Applied Mathematics*. 1951; 9(3): 225-236.
[39] Bhatt H, Khaliq A. Fourth-order compact schemes for the numerical simulation of coupled Burgers' equation. *Computer Physics Communications*. 2016; 200: 117-138. Available from: doi: 10.1016/j.cpc.2015.11.007.
[40] Fletcher C. Generating exact solutions of the two-dimensional Burgers' equations. *International Journal for Numerical Methods in Fluids*. 1983; 3: 213-216. Available from: doi: 10.1002/fld.1650030302.
[41] Kalita J. A super-compact higher order scheme for the unsteady 3D incompressible viscous flows. *Computational and Applied Mathematics*. 2014; 33(3): 717-738. Available from: doi: 10.1007/s40314-013-0090-y.
[42] Xu H, Matovic M, Pollard A. Finite difference schemes for three-dimensional time-dependent convection-diffusion equation using full global discretization. *Journal of Computational Physics*. 1997; 130(1): 109-122. Available from: doi: 10.1006/jcph.1996.5564.
[43] Saad Y. *Iterative methods for sparse linear systems*. Philadelphia: SIAM; 2003.
[44] Young D. *Iterative solution of large linear systems*. Amsterdam: Elsevier; 2014.
[45] Polyanin A. *Handbook of linear partial differential equations for engineers and scientists*. Boca Raton: CRC Press; 2001. Available from: doi: 10.1201/9781420035322.
[46] Qin J. The new alternating direction implicit difference methods for solving three-dimensional parabolic equations. *Applied Mathematical Modelling*. 2010; 34(4): 890-897. Available from: doi: 10.1016/j.apm.2009.07.006.
[47] Campos M, Romão E, Maura L. A finite-difference method of high-order accuracy for the solution of transient nonlinear diffusive-convective problem in three dimensions. *Case Studies in Thermal Engineering*. 2014; 3: 43-50. Available from: doi: 10.1016/j.csite.2014.03.001.
[48] Brüger A, Nilsson J, Kress W. A compact higher order finite difference method for the incompressible Navier–Stokes equations. *Journal of Scientific Computing*. 2002; 17(1): 551-560. Available from: doi: 10.1023/A:1015166529060.
[49] Lin P, Liu J, Lu X. Long time numerical solution of the Navier-Stokes equations based on a sequential regularization formulation. *SIAM Journal on Scientific Computing*. 2008; 31(1): 398-419. Available from: doi: 10.1137/060673722.

Appendix A

Values of expressions appear in equation (43).

P_1 $b[(q^3\Delta y_m^3 + r^3\Delta z_n^3)\Delta x_l - (q^2\Delta y_m^2 + r^2\Delta z_n^2)\Delta x_{l+1}]/[18\epsilon] - [24b\Delta x_{l+1}$
$+ p\Delta x_l\{p\Delta x_l^2(16b - 81\epsilon p^2\Delta x_l) - 96t\}]/[288\epsilon] + b\Delta t/[2\Delta x_l]$

P_2 $-\Delta t[b\Delta x_l^2\{bp\Delta x_l + (b - 4\epsilon p)\} + 12\epsilon^2]/[24\epsilon\Delta x_l^2] - (1 + p\Delta x_l)(bp\Delta x_l^2 - 2\epsilon)/[24\epsilon]$

P_3 $\Delta y_m[16c\{(p^3\Delta x_l^3 + r^3\Delta z_n^3) - q\Delta y_m(p^2\Delta x_l^2 + r^2\Delta z_n^2) - p^2\Delta x_l^2 - q^2\Delta y_m^2 - r^2\Delta z_n^2\}$
$+3q\Delta y_m(27\epsilon q^3\Delta y_m^2 - 8c) + 24(4\epsilon q - c)]/[288\epsilon] + c\Delta t/[2\Delta y_m]$

P_4 $-c\Delta t[c + q(c\Delta y_m - 4\epsilon)]/[24\epsilon] - (1 + q\Delta y_m)(cq\Delta y_m^2 - 2\epsilon)/[24\epsilon] - \epsilon\Delta t/[2\Delta y_m^2]$

P_5 $\Delta z_n[16d\{(p^3\Delta x_l^3 + q^3\Delta y_m^3) - r\Delta z_n(p^2\Delta x_l^2 + q^2\Delta y_m^2) - p^2\Delta x_l^2 - q^2\Delta y_m^2 - r^2\Delta z_n^2\}$
$-24d(1 + r\Delta z_n) + 3\epsilon r(32 + 27r^3\Delta z_n^3)]/[288\epsilon] + d\Delta t/[2\Delta z_n]$

P_6 $d\Delta t[4\epsilon r - d(1 + r\Delta z_n)]/[24\epsilon] - (1 + r\Delta z_n)(rd\Delta z_n^2 - 2\epsilon)/[24\epsilon] - \epsilon\Delta t/[2\Delta z_n^2]$

P_7 $[(\Delta x_{l+1}\Delta x_l + \Delta y_{m+1}\Delta y_m)c - 4\epsilon q\Delta y_m^2]\Delta t/[24\Delta x_l^2\Delta y_m]$

P_8 $[(\Delta x_{l+1}\Delta x_l + \Delta z_{n+1}\Delta z_n)d - 4\epsilon r\Delta z_n^2]\Delta t/[24\Delta x_l^2\Delta z_n]$

P_9 $[(\Delta x_{l+1}\Delta x_l + \Delta y_{m+1}\Delta y_m)b - 4\epsilon p\Delta x_l^2]\Delta t/[24\Delta x_l\Delta y_m^2]$

P_{10} $[(\Delta y_{m+1}\Delta y_m + \Delta z_{n+1}\Delta z_n)d - 4\epsilon r\Delta z_n^2]\Delta t/[24\Delta z_n\Delta y_m^2]$

P_{11} $[(\Delta x_{l+1}\Delta x_l + \Delta z_{n+1}\Delta z_n)b - 4\epsilon p\Delta x_l^2]\Delta t/[24\Delta x_l\Delta z_n^2]$

P_{12} $[(\Delta y_{m+1}\Delta y_m + \Delta z_{n+1}\Delta z_n)c - 4\epsilon q\Delta y_m^2]\Delta t/[24\Delta y_m\Delta z_n^2]$

P_{13} $-\epsilon[\Delta x_{l+1}\Delta x_l + \Delta y_{m+1}\Delta y_m]\Delta t_j/[24\Delta x_l^2\Delta y_m^2]$

P_{14} $-\epsilon[\Delta x_{l+1}\Delta x_l + \Delta z_{n+1}\Delta z_n]\Delta t_j/[24\Delta x_l^2\Delta z_n^2]$

P_{15} $-\epsilon[\Delta y_{m+1}\Delta y_m + \Delta z_{n+1}\Delta z_n]\Delta t_j/[24\Delta y_m^2\Delta z_n^2]$

P_{16} $[-(\Delta x_{l+1}\Delta x_l + \Delta y_{m+1}\Delta y_m)bc + 4\epsilon(bq\Delta y_m^2 + cp\Delta x_l^2)]\Delta t/[24\epsilon\Delta x_l\Delta y_m]$

P_{17} $[4\epsilon(dq\Delta y_m^2 + cr\Delta z_n^2) - (\Delta y_{m+1}\Delta y_m + \Delta z_{n+1}\Delta z_n)]\Delta t/[24\epsilon\Delta y_m\Delta z_n]$

P_{18} $[4\epsilon(dq\Delta x_l^2 + br\Delta z_n^2) - (\Delta x_{l+1}\Delta x_l + \Delta z_{n+1}\Delta z_n)]\Delta t/[24\epsilon\Delta x_l\Delta z_n]$

Q_1 $P_1 - b\Delta t/\Delta x_l$

Q_2 $-P_2 + (1 + p\Delta x_l)(2\epsilon - bp\Delta x_l^2)/[12\epsilon]$

Q_3 $P_3 - c\Delta t/\Delta y_m$

Q_4 $-P_4 + (1 + q\Delta y_m)(2\epsilon - cq\Delta y_m^2)/[12\epsilon]$

Q_5 $P_5 - d\Delta t/\Delta z_n$

Q_6 $-P_6 + (1 + r\Delta z_n)(2\epsilon - dr\Delta z_n^2)/[12\epsilon]$

Q_i $-P_i,\ i = 7(1)18$

$R_{l+1,m,n}$ $[\Delta x_l\{8b(q^2\Delta y_m^2 + r^2\Delta z_n^2) + p^2\Delta x_l^2(5b - 81\epsilon p) + 6(p\Delta x_l(b + 11\epsilon p) - 6\epsilon p + 2b)\} - 24\epsilon]\Delta t/(288\epsilon)$

$R_{l\text{-}1,m,n}$ $[\Delta x_l\{8b(q^2\Delta y_m^2 + r^2\Delta z_n^2) + 5p^2\Delta x_l^2(b + 3\epsilon p) + 6(p\Delta x_l(b - 5\epsilon p) - 6\epsilon p + 2b)\} + 24\epsilon]\Delta t/(288\epsilon)$

$R_{l,m+1,n}$ $[\Delta y_m\{8\epsilon(p^2\Delta x_l^2 + r^2\Delta z_n^2) + q^2\Delta y_m^2(5c - 81\epsilon q) + 6(q\Delta y_m(c + 11\epsilon q) - 6\epsilon p + 2c)\} - 24\epsilon]\Delta t/(288\epsilon)$

$R_{l,m\text{-}1,n}$ $-[\Delta y_m\{8c(p^2\Delta x_l^2 + r^2\Delta z_n^2) + 5q^2\Delta y_m^2(c + 3\epsilon q) + 6(q\Delta y_m(c - 5\epsilon q) - 6\epsilon p + 2c)\} + 24\epsilon]\Delta t/(288\epsilon)$

$R_{l,m,n+1}$ $[\Delta z_n\{8d(p^2\Delta x_l^2 + q^2\Delta y_m^2) + r^2\Delta z_n^2(5d - 81\epsilon r) + 6(r\Delta z_n(d + 11\epsilon r) - 6\epsilon r + 2d)\} - 24\epsilon]\Delta t/(288\epsilon)$

$R_{l,m,n\text{-}1}$ $-[\Delta z_n\{8d(p^2\Delta x_l^2 + q^2\Delta y_m^2) + 5r^2\Delta z_n^2(d + 3\epsilon r) + 6(r\Delta z_n(d - 5\epsilon r) - 6\epsilon r + 2d)\} + 24\epsilon]\Delta t/(288\epsilon)$

$R_{l,m,n}$ $[2p^2\Delta x_l^2(p\Delta x_l - 1) + 2q^2\Delta y_m^2(q\Delta y_m - 1) + 2r^2\Delta z_n^2(r\Delta z_n - 1) - 3]\Delta t/6$